Electronic Supplementary Material (ESI) for Journal of Materials Chemistry C.

Bionic Paired Hydrogen-Bond Strategy for Extending Organic π-Conjugation to Regulate Emission

Guigui Ye,[a, b] Yigang Wang,[a, b] Liming Hong,[c] Fuqing Yu,[c] Guomin Xia,*[a, b] and Hongming Wang*[a, b, c]

[a] Institute for Advanced Study, Nanchang University, 999, Xuefu Road, Nanchang, 330031, P.R. China
[b] School of Materials Science, Nanchang University, 999, Xuefu Road, Nanchang, 330031, P.R. China
[c] College of Chemistry, Nanchang University, 999, Xuefu Road, Nanchang, 330031, P.R. China

Content

1. Materials and instruments

All chemicals and solvents were purchased from commercial suppliers and used as received unless explicitly stated. ^{1}H NMR and ^{13}C NMR spectra were measured on a Bruker AVANCE 400 spectrometer in DMSO-d_6 (δ = 2.50 ppm) and $CDCl_3$ (δ = 7.26 ppm) using TMS as an internal standard. UV-visible absorption spectra were recorded on a Lambda 750 spectrophotometer. Photoluminescence (PL) spectra were recorded on a Horiba FluoroMax-4 luminescence spectrometer. The absolute PL quantum efficiencies (Φ_{PL}) were determined using a Horiba FL-3018 Integrating Sphere. The fluorescence lifetime measurement was performed on a Horiba FluoreCube spectrofluorometer system using a UV diode laser (NanoLED 375 nm) for excitation. SEM images were collected on a Hitachi S-4300 instrument. Mass spectra were obtained with X500R QTOF spectrometers. Thermogravimetric analysis (TGA) was carried out on a Dimand TG/DTA instrument at a heating rate of 10 ℃ min^{-1} under N_2 atmosphere. Powder X-ray diffraction (PXRD) data were collected using a SmartLab9KW X-ray diffractometer in parallel beam geometry employing CuKα radiation at 40 kV and 30 mA. The diffraction data were collected in the 2θ range from 5 to 30° at the scanning speed of 1.54 second per step with 2θ step increment of 0.02°. The X-ray diffraction experiments were carried out on a Bruker SMART APEX-II Single-crystal diffractometer at room temperature. All the structures were resolved and analyzed with the assistance of shelxl-97 software.

2. Syntheses

2.1 Synthesis of Pin-Ap

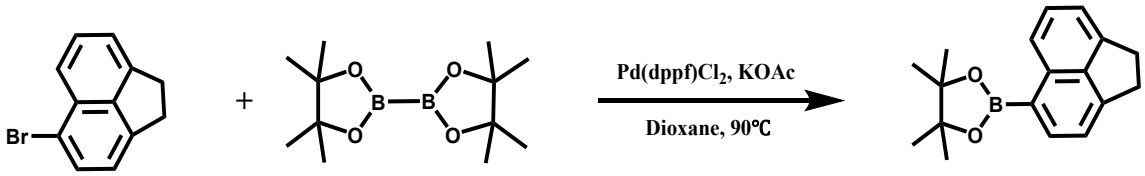

To dioxane (40 mL) were added 5-bromoacenaphthene (1.16 g, 5.00 mmol), bis(pinacolato)diboron (1.52 g, 6.00 mmol) and potassium acetate (1.76 g, 18.00 mmol) in the 100 ml radius flask. The mixture was purged with nitrogen flow for 30 min, and Pd(dppf)Cl_2 (226.61 mg, 0.31 mmol) was then added to the mixture. The reaction was stirred at 90 ℃ for 24 h under nitrogen. After cooling and removing most of the solvent in vacuum, the mixture was diluted with CH_2Cl_2 (200 mL). The organic phase was then washed with H_2O (400 mL) and saturated NaCl solution (50 mL). After dried over Na_2SO_4, the organic solvent was removed in vacuo. The crude product was purified via column chromatography (petroleum ether / dichloromethane = 80: 1) to give a white product **Pin-Ap** (1.01 g, 3.62 mmol, 72.35%). ^{1}H NMR (400 MHz, DMSO-d_6, δ): 8.20 (d, J = 8.36 Hz, 1H), 7.90 (d, J = 6.91 Hz, 1H), 7.47 (t, 1H), 7.29 (d, J = 7.01 Hz, 2H) 1.33 (s, 12H). ^{13}C NMR (100 MHz, DMSO-d_6, δ): 150.60, 146.34, 138.77, 137.93, 135.25, 128.74, 123.53, 119.70, 119.30, 83.70, 30.38, 30.08, 25.192.

2.2 Synthesis of TPE-Ap

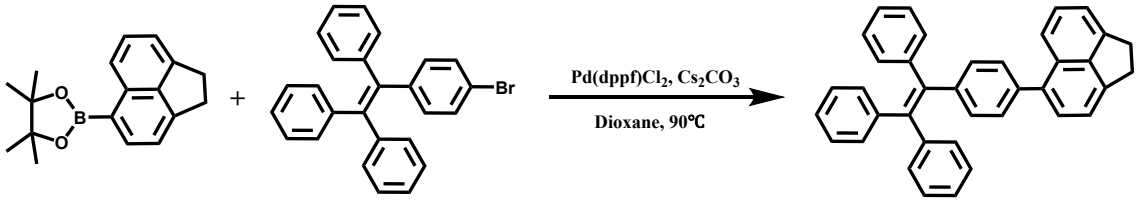

To dioxane (20 mL) were added Pin-Ap (280.16 mg, 1.00 mmol), 1-(4-Bromophenyl)-1,2,2-triphenylethylene (493.61 mg, 1.20 mmol), caesium carbonate (975.00 mg, 3.00 mmol), and H_2O (3 ml) in the 50 ml radius flask. The mixture was purged with nitrogen flow for 30 min, and $Pd(dppf)Cl_2$ (43.86 mg, 0.06 mmol) was then added to the mixture. The reaction was stirred at 90 ℃ for 12 h under nitrogen. After cooling and removing most of the solvent in vacuum, the mixture was diluted with CH_2Cl_2 (50 mL). The organic phase was then washed with H_2O (200 mL) and saturated NaCl solution (50 mL). After dried over Na_2SO_4, the organic solvent was removed in vacuo. The crude product was purified via column chromatography (petroleum ether / ethyl acetate = 50: 1) to give a white product **TPE-Ap** (329.55 mg, 0.68 mmol, 68.12%). ^{1}H NMR (400 MHz, $CDCl_3$, δ): 7.62 (d, J = 8.31 Hz, 1H), 7.39 (m, 2H), 7.31-7.27 (m, 4H), 7.19-6.97 (m, 17H), 3.43 (s, 4H). ^{13}C NMR (100 MHz, $CDCl_3$, δ): 146.14, 145.45, 143.80, 143.74, 142.33, 141.08, 140.77, 139.55, 138.35, 135.36, 131.45, 131.41, 131.38, 131.27, 129.67, 128.99, 128.38, 127.88, 127.69, 127.63, 126.46, 126.39, 120.85, 119.26, 119.06, 30.52, 29.99. HRMS (ESI) m/z: [TPE-Ap + H] $^+$ calcd for $C_{18}H_{28}$, 485.2264; found, 485.2231.

2.3 Synthesis of HTPE-Ap

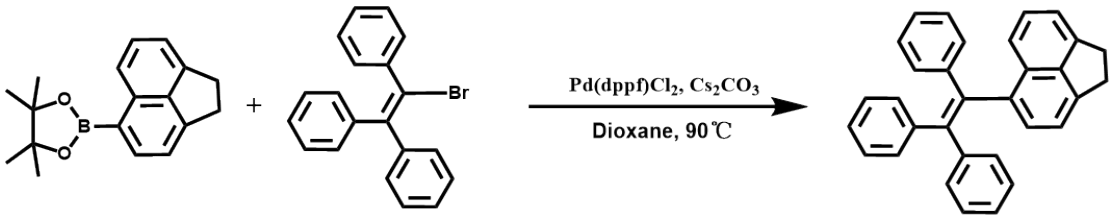

To dioxane (20 mL) were added Pin-Ap (280.16 mg, 1.00 mmol), 2-Bromo-1,1,2-triphenylethylene (402.29 mg, 1.20 mmol), caesium carbonate (975.00 mg, 3.00 mmol), and H_2O (3 ml) in the 50 ml radius flask. The reaction was stirred at 90 ℃ for 12 h under nitrogen. After cooling and removing most of the solvent in vacuum, the mixture was diluted with CH_2Cl_2 (50 mL). The organic phase was then washed with H_2O (200 mL) and saturated NaCl solution (50 mL). After dried over Na_2SO_4, the organic solvent was removed in vacuo. The crude product was purified via column chromatography (petroleum ether / ethyl acetate = 50: 1) to give a white product **HTPE-Ap** (253.29 mg, 0.62 mmol, 62.42%). ^{1}H NMR (400 MHz, $CDCl_3$, δ): 7.52 (d, *J* = 8.05 Hz 1H), 7.24-7.19 (m, 2H), 7.15 (d, *J* = 2.37 Hz, 5H), 7.08-6.99 (m, 6H), 6.94 (d, *J* = 13.17 Hz, 6H), 3.32 (m, 4H). ^{13}C NMR (100 MHz, $CDCl_3$, δ): 145.97, 145.23, 143.97, 143.55, 143.48, 142.56, 139.50, 139.18, 136.60, 131.53, 131.25, 130.66, 130.58, 130.32, 127.74, 127.60, 127.51, 127.31, 126.49, 126.22, 121.33, 118.83, 30.45, 29.99. HRMS (ESI) m/z: [HTPE-Ap + H] $^+$ calcd for $C_{32}H_{24}$, 409.1951; found, 409.1916.

2.4 Synthesis of Br-Np

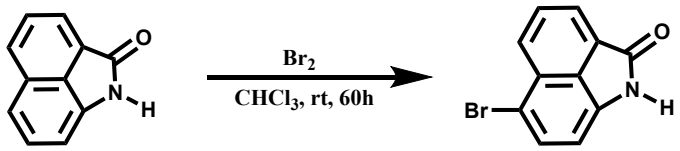

Br-Np was prepared according to the literature procedure.[1] Benz[c,d]indol-2(1H)-one (Np: 5.01 g, 29.10 mmol) was dissolved in chloroform (120 mL). Bromine (7.10 g, 44.40 mmol) was added to the solution and stirred at room temperature for 60 h. A saturated sodium thiosulfate aqueous solution (100 mL) was poured into the reaction mixture. The resulting precipitate was filtered off and washed with water to give crude product. The crude product was then purified via column chromatography (dichloromethane) to yield pale yellow product Np-Br (5.85 g, 23.58 mmol, 81%). ^{1}H NMR (400 MHz, DMSO- d_6, δ): 10.91 (s, 1H), 8.19-8.04 (m, 2H), 7.93 (t, J = 8.12 Hz, 1H), 7.76 (d, J = 7.54 Hz, 1H), 6.93 (d, J = 8.25 Hz, 1H). ^{13}C NMR (100 MHz, DMSO-d_6, δ): 168.61, 138.55, 132.31, 130.88, 129.98, 128.81, 127.79, 127.11, 125.26, 112.31, 107.91.

2.5 Synthesis of Pin-Np

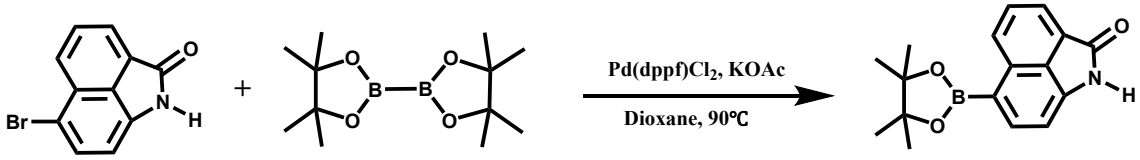

To dioxane (40 mL) were added Br-Np (1.24 g, 5.00 mmol), bis(pinacolato)diboron (1.52 g, 6.00 mmol) and potassium acetate (1.76 g, 18.00

mmol) in the 100 ml radius flask. The mixture was purged with nitrogen flow for 30 min, and Pd(dppf)Cl_2 (226.61 mg, 0.31 mmol) was then added to the mixture. The reaction was stirred at 90 ℃ for 24 h under nitrogen. After cooling and removing most of the solvent in vacuum, the mixture was diluted with CH_2Cl_2 (200 mL). The organic phase was then washed with H_2O (400 mL) and saturated NaCl solution (50 mL). After dried over Na_2SO_4, the organic solvent was removed in vacuo. The crude product was purified via column chromatography (dichloromethane / ethyl acetate = 50: 1) to give a pale-yellow product **Pin-Np** (1.95 g, 0.66 mmol, 66.00%). ^{1}H NMR (400 MHz, DMSO-d_6, δ): 10.90 (s, 1H), 8.63 (d, J = 8.15 Hz, 1H), 7.99-7.93 (m, 2H), 7.83-7.79 (m, 1H), 6.98 (d, J = 7.14 Hz, 1H), 1.38 (s, 12H), ^{13}C NMR (100 MHz, DMSO-d_6, δ): 169.34, 141.66, 139.53, 132.73, 132.34, 129.72, 127.16, 125.96, 124.06, 106.12, 83.88, 25.17.

2.6 Synthesis of TPE-Np

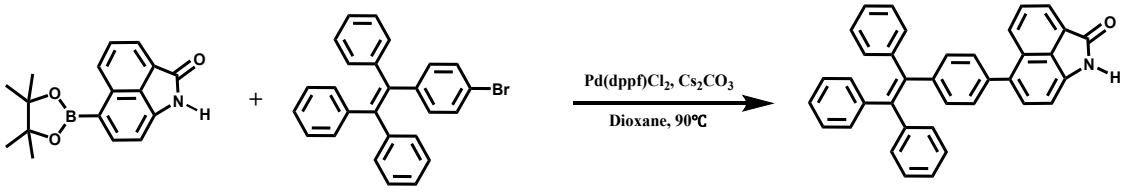

To dioxane (20 mL) were added Pin-Np (295 mg, 1.00 mmol), 1-(4-Bromophenyl)-1,2,2-triphenylethylene (493.61 mg, 1.20 mmol), caesium carbonate (975.00 mg, 3.00 mmol), and H_2O (3 ml). The mixture was purged with nitrogen flow for 30 min, and Pd(dppf)Cl_2 (43.90 mg, 0.06 mmol) was then added to the mixture.

The reaction was stirred at 90℃ for 12 h under nitrogen. After cooling and removing most of the solvent in vacuum, the mixture was diluted with CH_2Cl_2 (50 mL). The organic phase was then washed with H_2O (200 mL) and saturated NaCl solution (50 mL). After dried over Na_2SO_4, the organic solvent was removed in vacuo. The crude product was purified via column chromatography (dichloromethane) to give a yellow product **TPE-Np** (313.46 mg, 0.63 mmol, 62.74%). ^{1}H NMR (400 MHz, DMSO-d_6, δ): 10.83 (s, 1H), 8.01 (m, 2H), 7.79 (t, 1H), 7.39 (d, J = 7.14 Hz, 1H), 7.31 (d, J = 8.02 Hz, 2H), 7.17-6.97 (m, 19H). ^{13}C NMR (100 MHz, DMSO-d_6, δ): 169.15, 143.59, 143.54, 142.54, 141.35, 140.60, 138.01, 137.12, 132.38, 131.44, 131.16, 131.09, 129.76, 129.70, 129.50, 129.30, 128.37, 128.35, 128.26, 127.69, 127.53, 127.12, 127.06, 127.02, 126.24, 124.28, 106.80. HRMS (ESI) m/z: [TPE-Np + H] $^+$ calcd for $C_{37}H_{25}NO$, 500.2009; found, 500.2008.

2.7 Synthesis of HTPE-Np

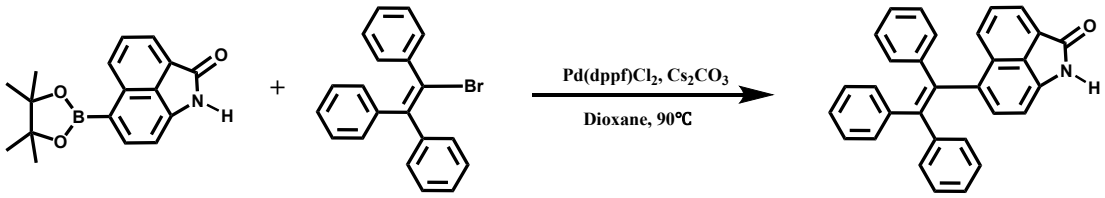

To dioxane (20 mL) were added Pin-Np (295.00 mg, 1.00 mmol), 2-Bromo-1,1,2-triphenylethylene (402.29 mg, 1.2 mmol), caesium carbonate (975.00 mg, 3.00 mmol), and H_2O (3 ml). The mixture was purged with nitrogen flow for 30 min, and Pd(dppf)Cl_2 (43.90 mg, 0.06 mmol) was then added to the mixture. The reaction was

stirred at 90℃ for 12 h under nitrogen. After cooling and removing most of the solvent in vacuum, the mixture was diluted with CH_2Cl_2 (50 mL). The organic phase was then washed with H_2O (200 mL) and saturated NaCl solution (50 mL). After dried over Na_2SO_4, the organic solvent was removed in vacuo. The crude product was purified via column chromatography (dichloromethane) to give a yellow product **HTPE-Np** (255.90 mg, 0.60 mmol, 60.33%). ^{1}H NMR (400 MHz, DMSO-d_6, δ): 10.71 (s, 1H), 7.98 (d, J = 8.21 Hz, 1H), 7.89 (d, J = 6.92 Hz, 1H), 7.62 (m, 1H), 7.22-7.16 (m, 4H), 7.12-7.01 (m, 7H), 6.98-6.93 (m, 5H), 6.82 (d, J = 7.27 Hz, 1H). ^{13}C NMR (100 MHz, DMSO-d_6, δ): 169.22, 143.80, 143.68, 143.31, 138.05, 137.72, 134.49, 132.07, 131.29, 130.58, 130.36, 130.13, 129.26, 128.71, 128.44, 128.36, 128.08, 127.50, 127.25, 127.03, 126.93, 126.15, 123.91, 106.61. HRMS (ESI) m/z: [HTPE-Np + H] $^+$ calcd for $C_{31}H_{21}NO$, 424.1696; found, 424.1684.

3. Photophysical data in solution

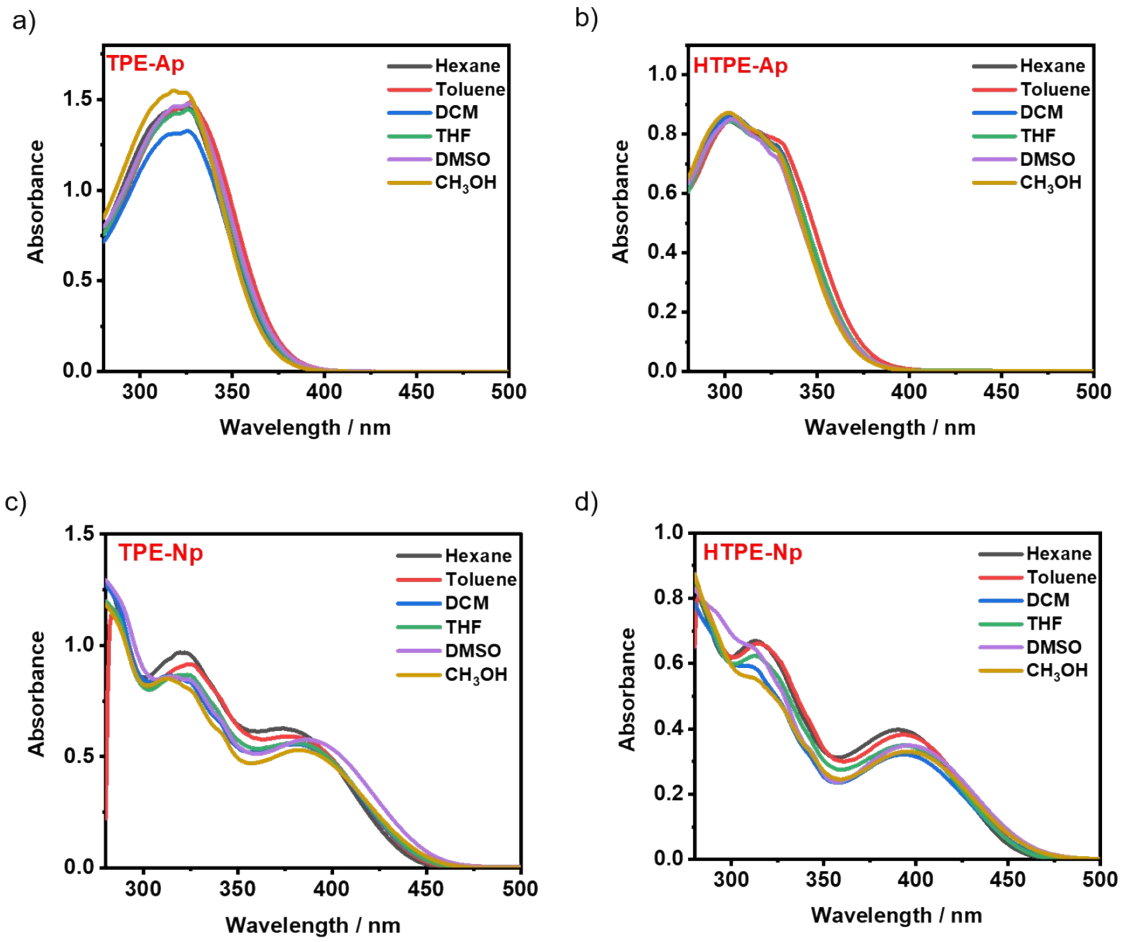

Figure S1. Absorption spectra of a) **TPE-Ap**, b) **HTPE-Ap**, c) **TPE-Np** and d) **HTPE-Np** (50 μM) in different solvents.

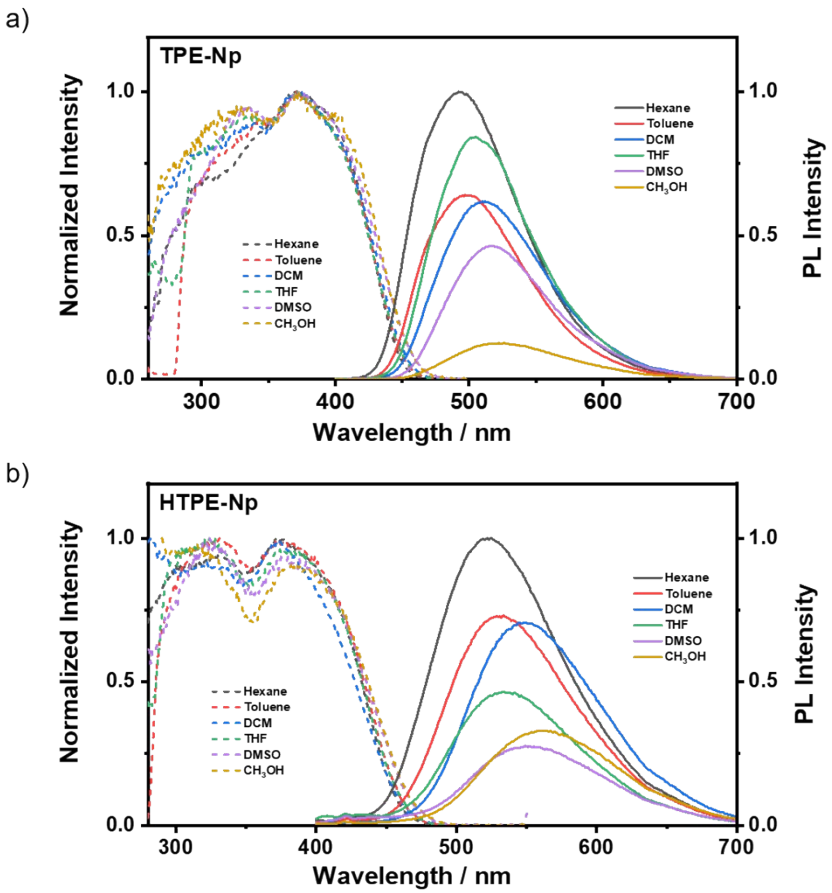

Figure S2. The excitation spectra (dotted line) and PL spectra (solid line) of a) **TPE-Np** and b) **HTPE-Np** (50 μM) in different solvents solutions.

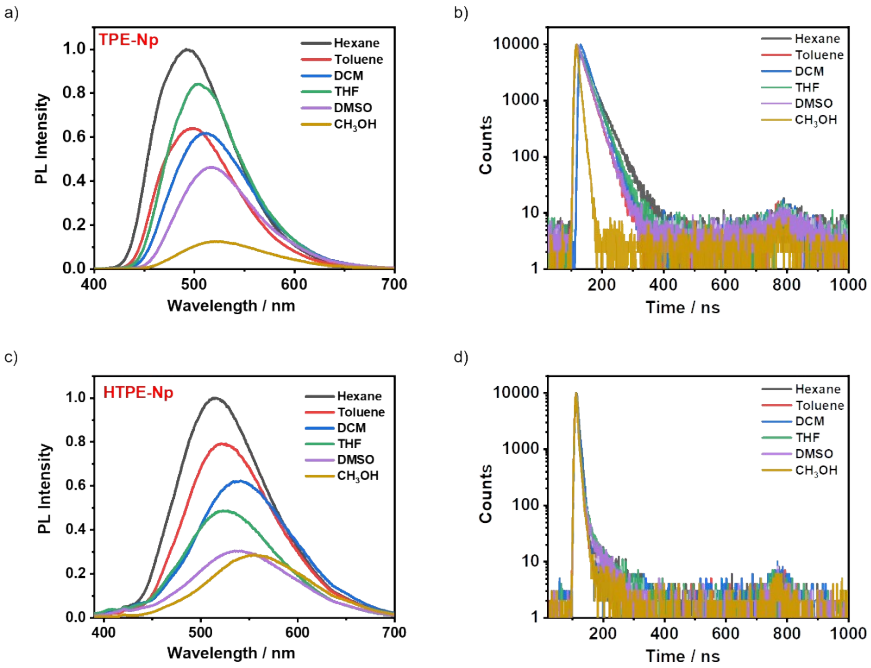

Figure S3. PL spectra of a) **TPE-Np** and b) **HTPE-Np**, and fluorescence decay profiles of c) **TPE-Np** and d) **HTPE-Np** (50 μM) in different solvents, λ_{ex} = 375 nm.

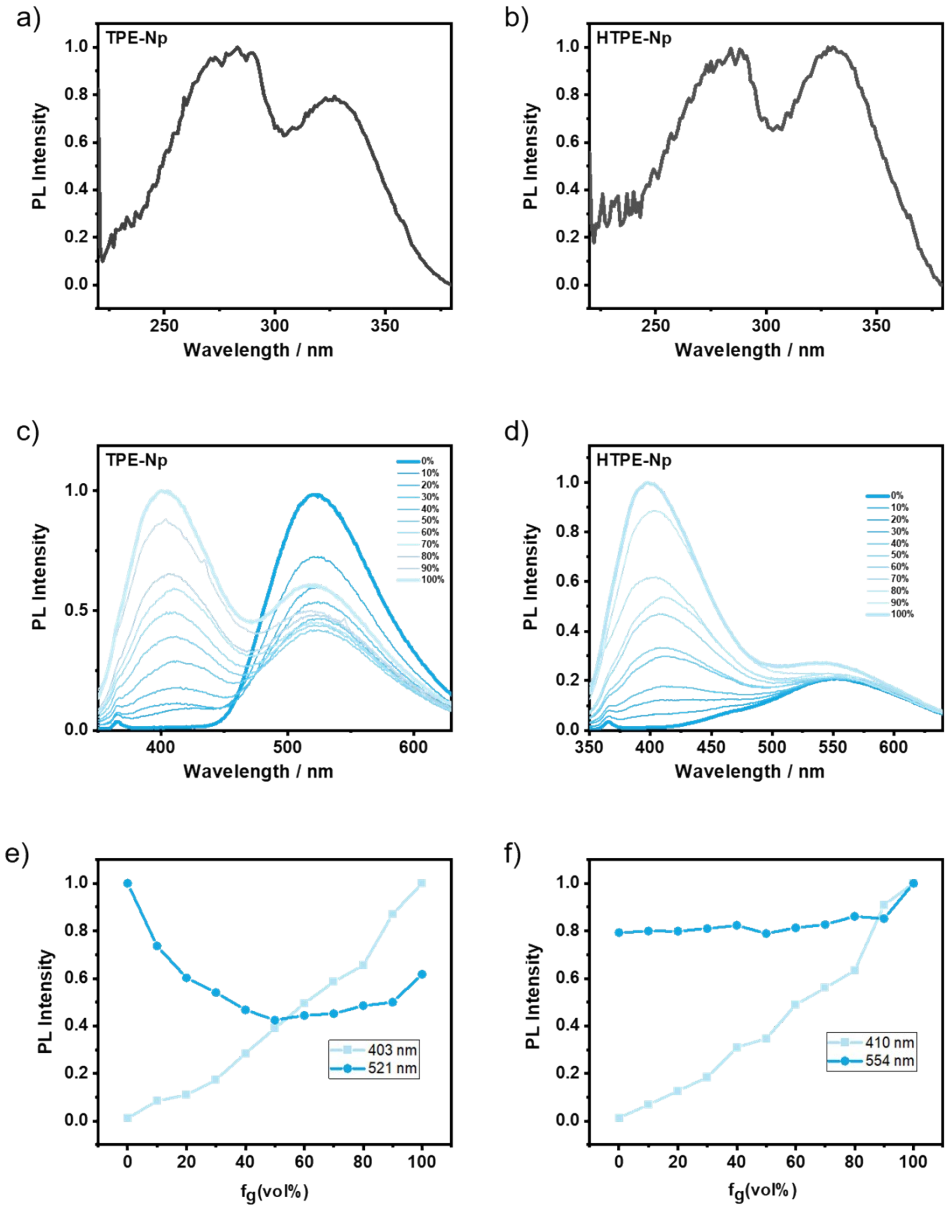

Figure S4. The excitation spectrum of a) **TPE-Np** (10 μM) and b) **HTPE-Np** (10 μM) in pure glycerol; The PL spectra changes of c) **TPE-Np** (10 μM, λ_{ex} = 325 nm) and d) **HTPE-Np** (10 μM, λ_{ex} = 330 nm) in methanol/glycerol mixtures with different fractions of glycerol (f_g, by volume) at room temperature; plots of corresponding maximum fluorescence intensity of e) **TPE-Np** and f) **HTPE-Np** vs. % glycerol.

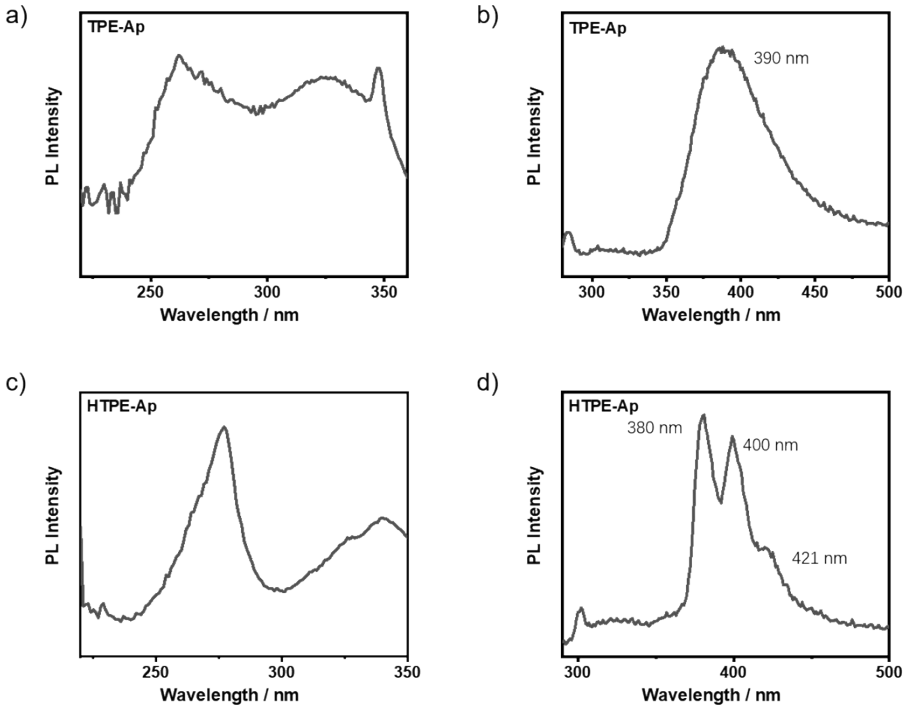

Figure S5. The excitation spectrum of a) TPE-Ap (50 μM) and c) HTPE-Ap (50 μM) in pure THF; The PL spectrum of b) TPE-Ap (50 μM, λ_{ex} = 262) and d) HTPE-Ap (50 μM, λ_{ex} = 277) in pure THF.

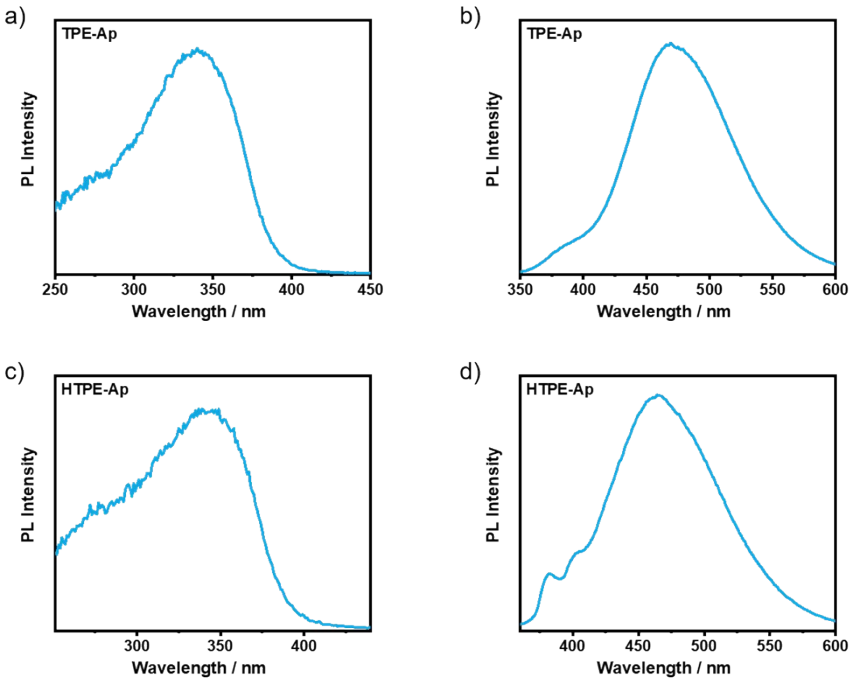

Figure S6. The excitation spectrum of a) TPE-Ap (10 μM) and c) HTPE-Ap (10 μM) in pure THF; The PL spectrum of b) TPE-Ap (10 μM, λ_{ex} = 339 nm) and d) HTPE-Ap (10 μM, λ_{ex} = 345 nm) in pure glycerol.

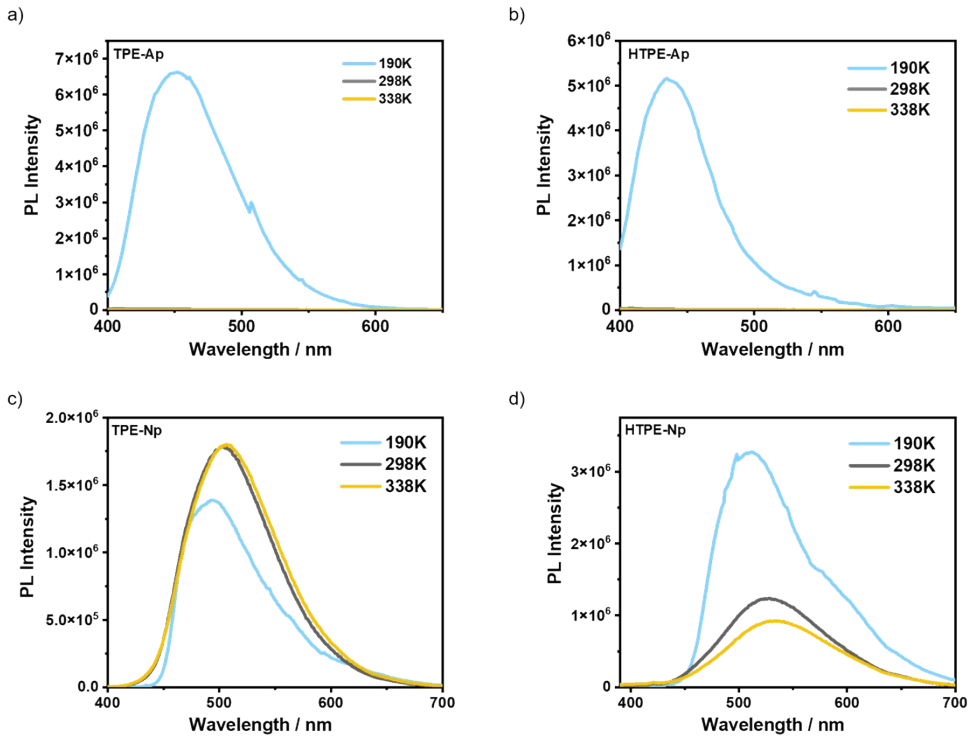

Figure S7. PL spectra of a) **TPE-Ap,** b) **HTPE-Ap**, c) **TPE-Np** and d) **HTPE-Np (**50 μM**)** in THF at different temperature, λ_{ex} = 375 nm.

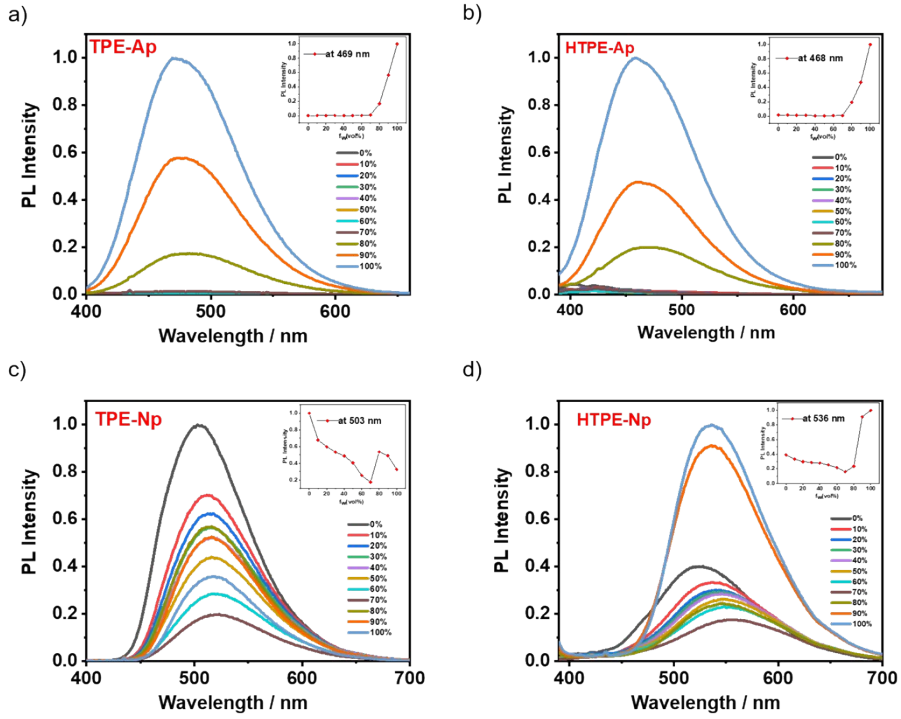

Figure S8. PL spectra of a) **TPE-Ap**, b) **HTPE-Ap**, c) **TPE-Np** and d) **HTPE-Np** (50 μM) in THF solution with different fractions of water (f_w) at room temperature, λ_{ex} = 375 nm. Inset: plots of corresponding maximum fluorescence intensity vs. % H_2O.

Table S1. The photophysical data for **TPE-Np** and **HTPE-Np** in solution (50 μM) at 298 K.

Condition		λ_{abs} [nm]	λ_{em} [a)] [nm]	Φ_{PL} [b)] [%]	τ_f [c)] [ns]		X^2	k_f [d)] [10^7 s^{-1}]	k_{nr} [e)] [$10^7 s^{-1}$]
TPE-Np	Hexane	321/378	494	51.84	τ_1=3.45 α_1=13.37 τ_2=7.40 α_2=86.63	7.49	1.04	6.92	6.43
	Toluene	324/383	498	44.22	τ_1=4.21 α_1=34.89 τ_2=5.64 α_2=65.11	5.37	1.08	8.23	10.39
	CH_2Cl_2	323/381	512	41.65	τ_1=5.00 α_1=92.41 τ_2=7.26 α_2=7.59	5.20	1.02	8.01	11.22
	THF	325/384	505	49.08	τ_1=4.81 α_1=17.41 τ_2=6.38 α_2=82.59	6.19	1.08	7.93	8.23
	DMSO	324/390	518	27.32	τ_1=8.29 α_1=1.27 τ_2=5.21 α_2=98.73	5.22	1.06	5.23	13.92
	CH_3OH	323/385	524	12.51	τ_1=0.34 α_1=5.21 τ_2=1.51 α_2=94.79	1.45	1.03	8.63	60.34
HTPE -Np	Hexane	313/391	523	24.35	τ_1=0.95 α_1=98.14 τ_2=11.00 α_2=1.86	1.13	1.02	21.55	66.95
	Toluene	319/403	533	20.86	τ_1=0.79 α_1=95.24 τ_2=2.81 α_2=4.76	0.88	1.02	23.70	89.93
	CH_2Cl_2	316/402	551	18.69	τ_1=0.97 α_1=92.41 τ_2=2.48 α_2=7.59	1.08	1.05	17.31	75.29
	THF	311/395	534	14.02	τ_1=0.64 α_1=95.36 τ_2=6.40 α_2=4.64	0.91	1.04	15.41	94.48
	DMSO	311/398	549	8.79	τ_1=0.61 α_1=96.99 τ_2=7.90 α_2=3.01	0.83	1.05	10.59	109.89
	CH_3OH	313/398	560	7.88	τ_1=0.64 α_1=98.91 τ_2=4.96 α_2=1.09	0.68	1.00	11.59	135.47

a) λ_{ex} = 375 nm in **TPE-Np** and **HTPE-Np** orderly; b) Measured using an integrating sphere method; c) Measured using a method of double-exponential decay; d) Radiative rate constant ($k_f = \Phi_f / \tau_f$); e) Nonradiative rate constant ($k_{nr} = (1-\Phi_f) / \tau_f$).

4. Crystal study

4.1 Preparations and characterizations of single crystalline assemblies

TPE-Ap crystal: The single crystal of TPE-Ap was attained by slowly vaporizing their corresponding mixtures of THF / EtOH (1: 3, v/v), and its morphology was white bulk.

HTPE-Ap crystal: The single crystal of HTPE-Ap was attained by slowly vaporizing in corresponding mixtures THF / EtOH (1: 3, v/v), and its morphology was white bulk.

TPE-Np crystal: The single crystal of TPE-Np was attained by slowly vaporizing their corresponding mixtures of THF / EtOH (1: 3, v/v), and its morphology was yellowish-green bulk.

HTPE-Np crystal: The single crystal of HTPE-Np was attained by slowly vaporizing their corresponding mixtures of THF / EtOH (1: 3, v/v), and its morphology was yellowish-green bulk.

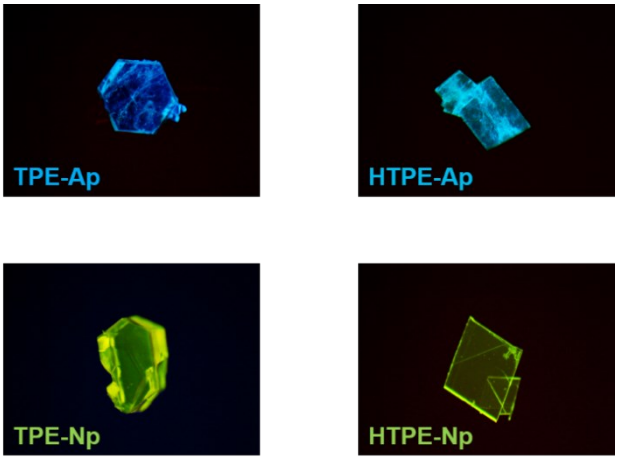

Figure S9. The corresponding luminescence photographs of single crystal of **TPE-Ap**, **HTPE-Ap**, **TPE-Np** and **HTPE-Np** under 365 nm UV lamp.

4.2 Crystal data

Table S2. Crystallographic data of **TPE-Ap**, **HTPE-Ap**, **TPE-Np** and **HTPE-Np.**

Sample	TPE-Ap	HTPE-Ap	TPE-Np	HTPE-Np
CCDC number	2054774	2054775	2054872	2022585
Empirical formula	$C_{38}H_{28}$	$C_{32}H_{24}$	$C_{37}H_{25}NO$	$C_{31}H_{21}NO$
Formula weight	484.06	408.51	499.58	423.49
***T* [K]**	293(2)	293(2)	293(2)	293(2)
Crystal system	Monoclinic	Monoclinic	Triclinic	Triclinic
Space group	C2/c	P21/c	P-1	P-1
a **[Å]**	15.964	7.835	9.018(3)	7.589
b **[Å]**	9.246	19.144	9.602(4)	9.245
c **[Å]**	36.716	5.286	17.214(8)	16.946
α **[°]**	90.000	90.000	96.738(4)	93.590(5)
β **[°]**	94.762(3)	97.395	96.835(3)	91.639(5)
γ **[°]**	90.000	90.000	94.726(3)	102.653(3)
V **[Å^3]**	828.7(2)	2273.74(13)	1462.57(11)	1156.72(11)
Z	8	4	2	2
F(000)	2376	848	638	444
Density [g/cm^3]	1.192	1.182	1.134	1.216
μ **[mm^{-1}]**	0.067	0.067	0.067	0.073
Reflections collected	28152	29979	24414	21014
Unique reflections	4708	3999	5130	4050
***R* (int)**	0.0292	0.0250	0.0264	0.0606
GOF	1.650	2.371	2.531	3.048
***R_1* [*I*>2σ(*I*)]**	0.0659	0.0696	0.1216	0.1601
***ωR_2* [*I*>2σ(*I*)]**	0.2179	0.2169	0.3572	0.4291
***R_1* (all data)**	0.0729	0.0801	0.1448	0.1680
***ωR_2* (all data)**	0.2223	0.2217	0.3689	0.4324

4.3 Crystal structure analysis

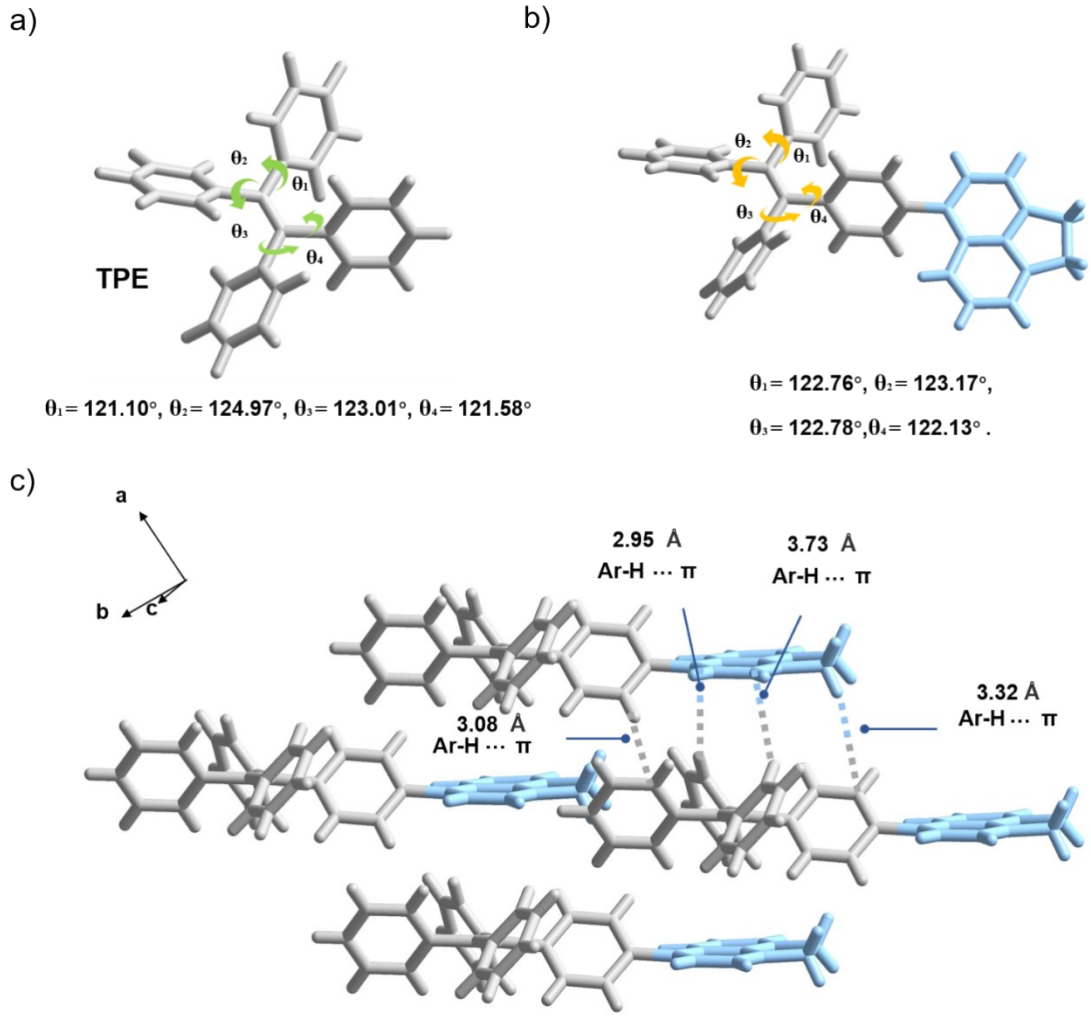

Figure S10. a) Structure of TPE, b) Structure and c) molecular stacking in TPE-Ap crystal

TPE-Ap crystal belonged to monoclinic crystal system and crystallized in the space group of C2/c with eight TPE-Ap molecules in one unit cell taking the parameters of a = 15.964 Å, b = 9.246 (11) Å and c = 36.716 Å. As compared to TPE molecule, the dihedral angles between vinyl bond and phenyl rotors exhibited slight change for θ_1 from 122.76° to 121.10°, θ_2 from 123.17° to 124.97°, θ_3 from 122.78° to 123.01° and θ_4 from 122.13° to 121.58°, respectively, in TPE-Ap molecule. It was noteworthy that multiple intermolecular hydrogen bonds served to the packing model

with avoiding π-stacking and locked rotated phenyl rings on tetraphenylethylene. As shown in Figure S6c, three types of moderate Ar-H···π hydrogen bond between Ar-H and π electron in adjacent acenaphthene were observed in 2.95 Å, 3.32 Å, and 3.73 Å, and the another one was in 3.08 Å between Ar-H and adjacent phenyl rings. Accordingly, the stacking mode in TPE-Ap crystal was particularly similar to that TPE ones, indicating that their consistent emission behavior in aggregated states.

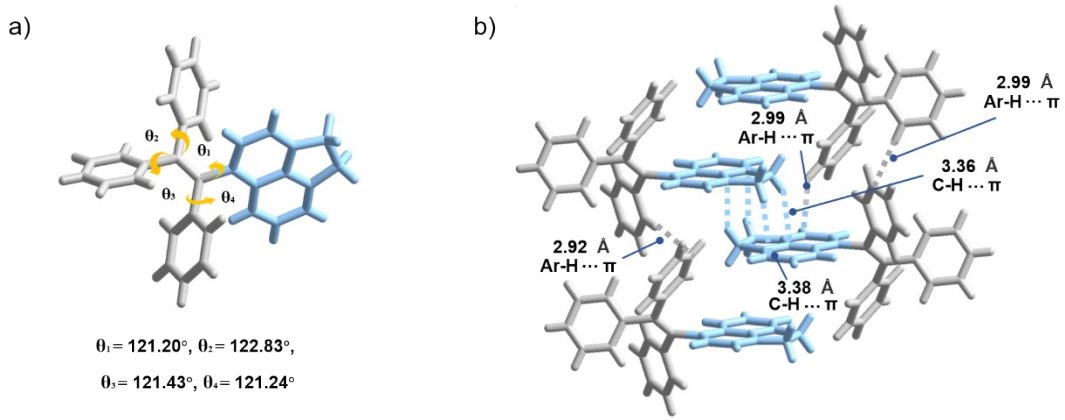

Figure S11. a) Structure and b) molecular stacking in HTPE-Ap crystal

HTPE-Ap crystal belonged to triclinic crystal system and crystallized in the space group of P-1 with two HTPE-Ap molecules in one unit cell taking the parameters of a = 7.835 Å, b = 19.144 Å and c = 5.286 Å. Similar to TPE-Ap molecule, the dihedral angles between vinyl bond and phenyl rotors exhibited θ_1 =121.20°, θ_2=122.83°, θ_3 =121.43° and θ_4 =121.24°, respectively, in HTPE-Ap molecule. Instead of π-π interaction, the two C-H···π intermolecular hydrogen bond in 3.36 Å and 3.38 Å played a main role between two adjacent aromatic planes. Importantly, the three rotated phenyl rings were restrained by two type of Ar-H···π hydrogen bonding interaction, showing 2.99 Å and 2.92 Å between Ar-H and π

electron in phenyl ring and 2.99 Å between Ar-H and acenaphthene. As the results, HTPE-Ap could be efficiently emissive in solid state, showing AIE characteristic.

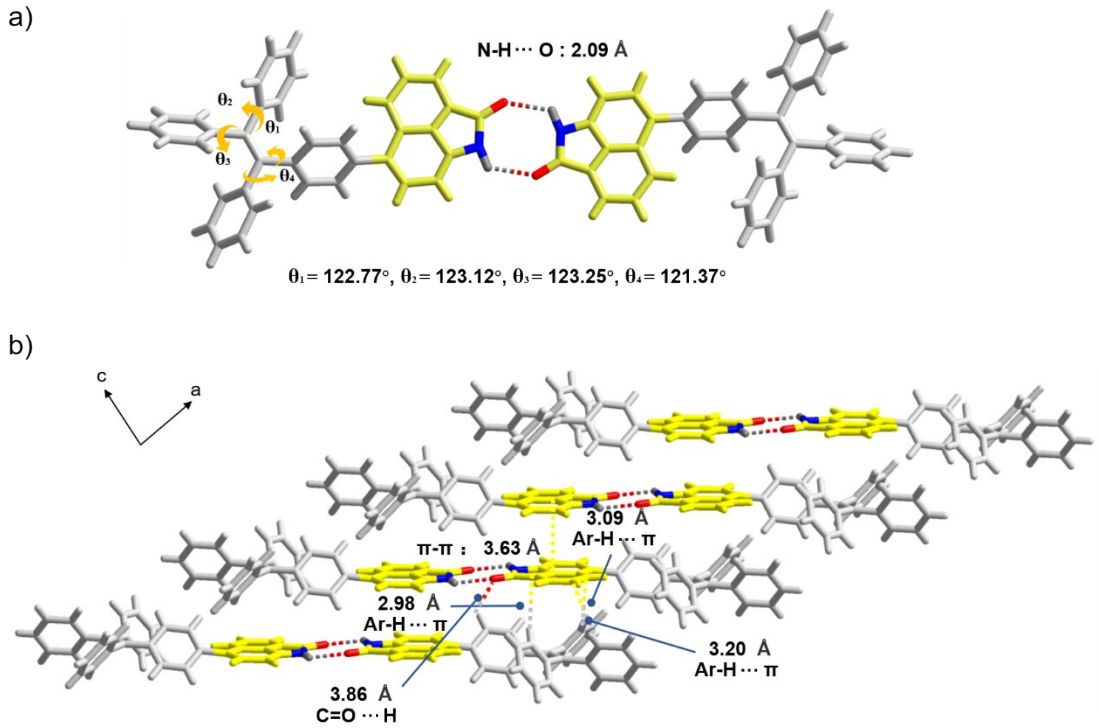

Figure S12. a) Structure and b) molecular stacking in TPE-Np crystal.

TPE-Np crystal belonged to triclinic crystal system and crystallized in the space group of P-1 with two TPE-Np molecules in one unit cell taking the parameters of a = 9.018(3) Å, b = 9.602(4) Å and c = 17.214(8) Å. The dihedral angles between vinyl bond and phenyl rotors exhibited θ_1 =122.77°, θ_2=123.12°, θ_3 =123.25° and θ_4 =121.37°, respectively, in TPE-Np molecule. Obviously, strong intramolecular N-H···O hydrogen bond in 2.09 Å was observed between the TPE-Np dimers, therefore they could reasonably be regarded as a single unit to be analyzed and discussed. Owing to the strong intramolecular N-H···O hydrogen bond, the discrete π-π interaction in 3.63 Å and J-stacking were formed along a, c-axis. Besides, there were another two types of hydrogen bond to lock the free phenyl rings. One type was Ar-

H···π in 2.98 Å, 3.09 Å and 3.20 Å between Ar-H and π electron in phenyl ring, the other one was C=O···H in 3.68 Å between carbonyl in 1,8-naphtholactam and hydrogen atom in tetraphenylethylene. Therefore, the TPE-Np not only inherited the good performance of AIE precursors, but also improved the rigidity of molecule by hydrogen bonds. These factors contributed to efficient emission in solution and solid state.

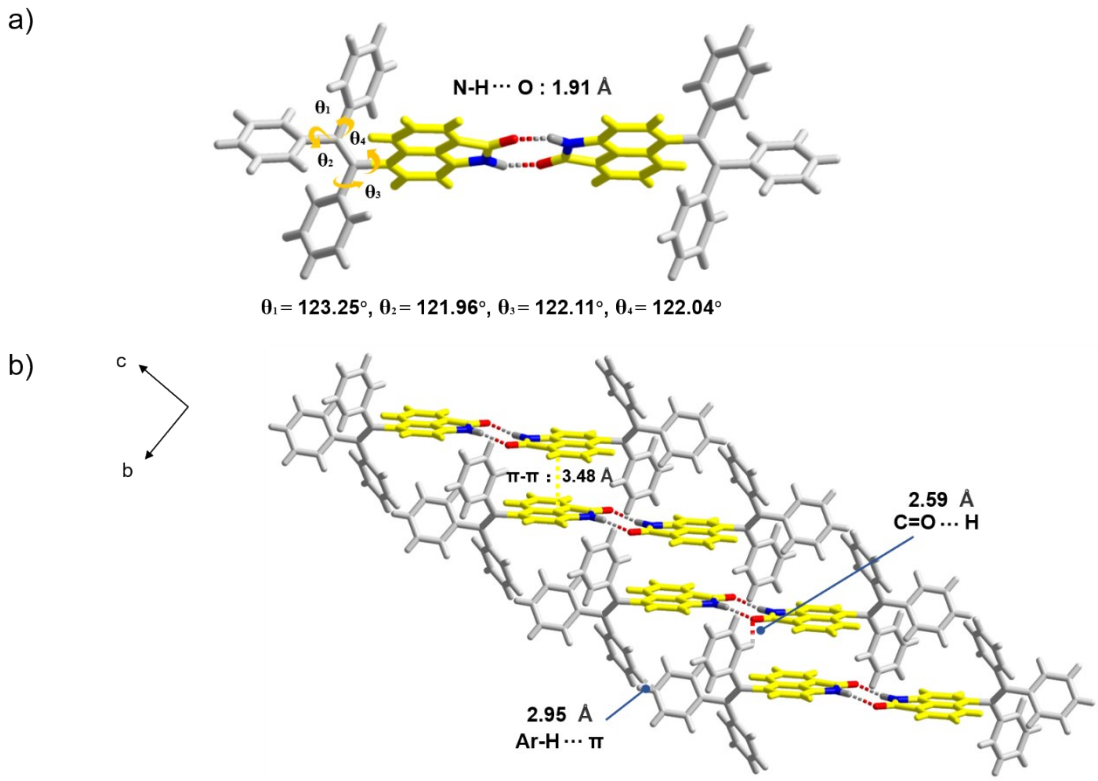

Figure S13. a) Structure and b) molecular stacking in HTPE-Np crystal.

HTPE-Np crystal belonged to triclinic crystal system and crystallized in the space group of P-1 with two HTPE-Np molecules in one unit cell taking the parameters of a = 7.589 Å, b = 9.245 Å and c = 16.946 Å. The dihedral angles between vinyl bond and phenyl rotors exhibited θ_1 =123.25°, θ_2 = 121.96°, θ_3 = 122.11° and θ_4 = 122.04°, respectively, in HTPE-Np molecule. Similar to TPE-Np,

strong intramolecular N-H···O hydrogen bond in 1.91 Å were also observed between the HTPE-Np dimers. Similarly, the discrete π-π interaction in 3.48 Å and J-stacking were also formed along b, c-axis. The free phenyl rings of HTPE-Np were restrained by C=O···H and Ar-H···π hydrogen bonds (2.59 Å and 2.95 Å). Therefore, the TPE-Np not only inherited the good performance of AIE precursors, but also improved the rigidity of molecule by hydrogen bonds. The HTPE-Np crystal could be efficiently emissive in solution and solid state.

4.4 Preparations and characterizations of microcrystalline assemblies

All the microstructures (TPE-Ap, HTPE-Ap, TPE-Np and HTPE-Np) were prepared via a liquid phase self-assembly method, 1 mmol compounds was completely dissolved in the 4 mL refluxing THF/ EtOH (volume ratio is 1:3) solution with vigorous sonication for 10 min. After cooling and aging in closed tubes at room temperature for 25 min, the corresponding assemblies with suitable dimensions were formed in the solutions. These microstructures were then used to prepare samples for further characterizations.

As shown, PL microscopy and scanning electron microscopy (SEM) images revealed that the assembly of **HTPE-Ap, TPE-Np** and **HTPE-Np** yielded oblong block with edge lengths of about 6 to 50 μm μm and widths around around 5 to 30μm. Moreover, **TPE-Ap**, different from other compouds, showed nanoparticles of hexagon block with six edge lengths around 6 μm. Furthermore, power X-ray diffraction (PXRD) patterns of these pristine crystalline powders showed sharp and intense peaks, indicating good microcrystalline structures. The simulated XRD patterns of crystals turned out to be coincided with that of their crystalline assemblies (Figure S14), suggesting the same molecular packing modes. Thermogravimetric analysis (TGA) experiments revealed that these microstructures were stable until ≈ 310 ℃ with the exception of HTPE-Ap assemblies (Figure S15a, c and d), which was stable until 239.54 ℃ (Figure S15b).

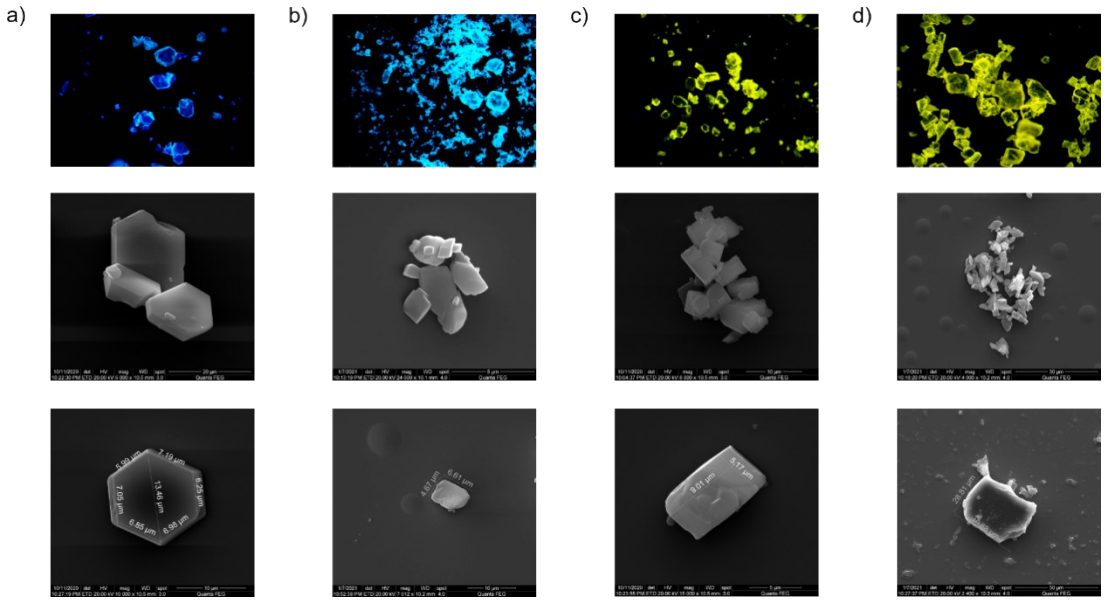

Figure S14. Photographs of a) **TPE-Ap**, b) **HTPE-Ap**, c) **TPE-Np**, and d) **HTPE-Np** in crystalline assemblies taken under 365 nm UV illumination and SEM.

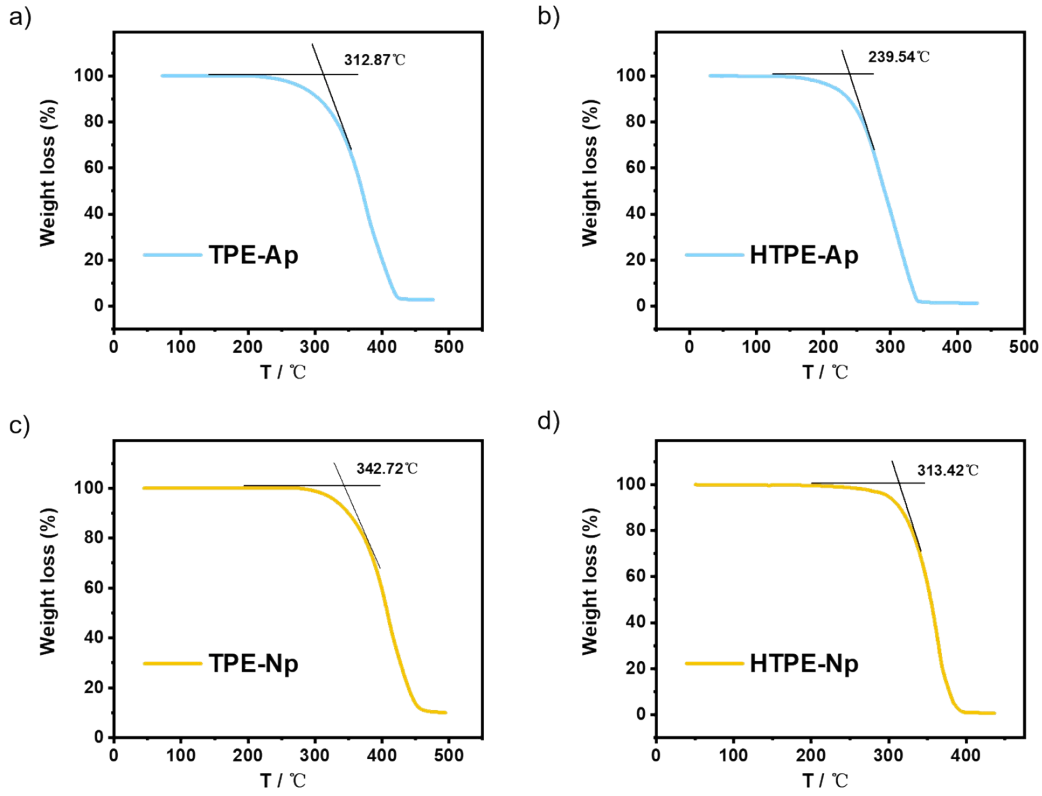

Figure S15. TGA curves of pristine a) **TPE-Ap**, b) **HTPE-Ap**, c) **TPE-Np**, and d) **HTPE-Np** assemblies at heating rate of 10 ℃ min^{-1} under N_2 atmosphere.

4.5 Date of XRD

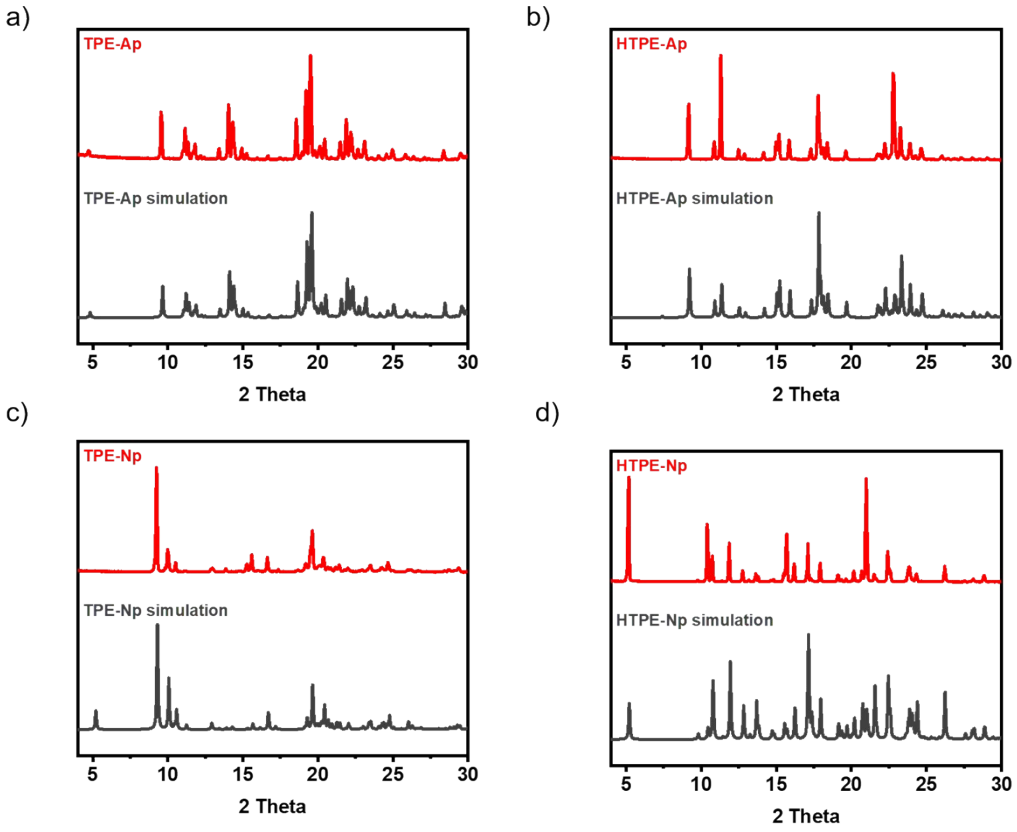

Figure S16. The PXRD of the a) **TPE-Ap**, b) **HTPE-Ap**, c) **TPE-Np**, and d) **HTPE-Np** microcrystals.

4.6 Photophysical data in crystal

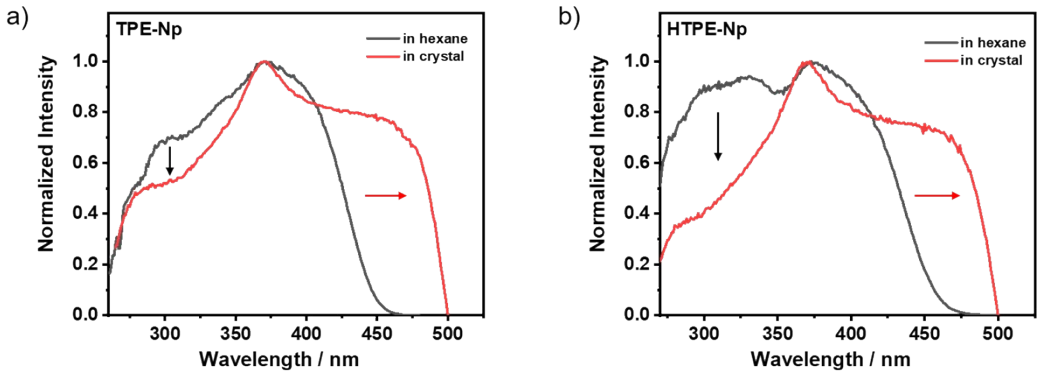

Figure S17. The excitation spectra of a) **TPE-Np** and b) **HTPE-Np** in hexane solutions (50 μM) and crystals**.**

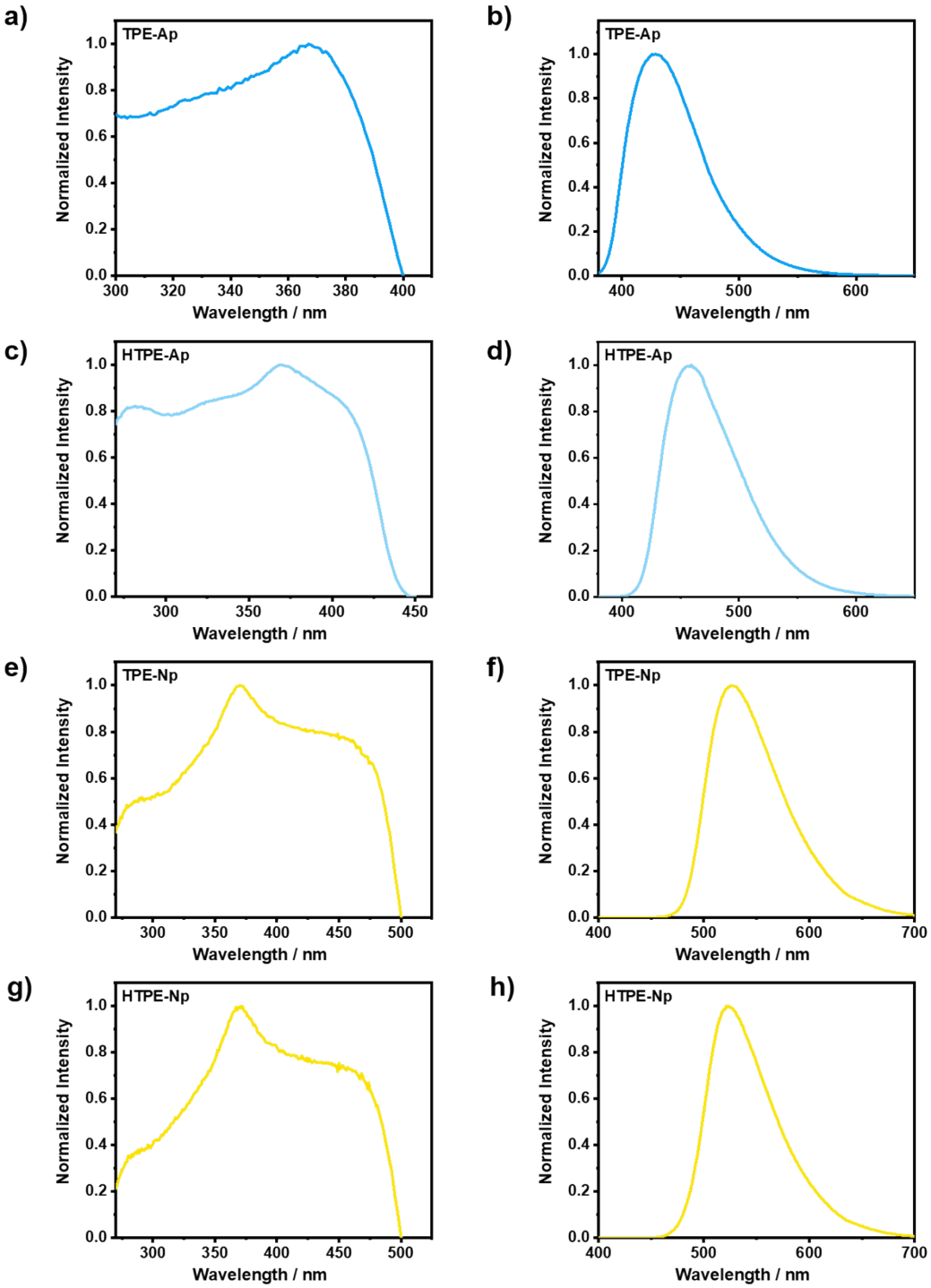

Figure S18. The excitation and PL spectra of a, b) TPE-Ap, c, d) HTPE-Ap, e, f) TPE-Np and g, h) HTPE-Np crystals.

5. The computational details

All the geometrical optimizations and frequency calculations were carried out using the (TD)B3LYP/6-311G(d, p) at the S_0 (S_1) for the studied compounds[2-4].The solution phase was taken into account through the polarizable continuum model (PCM). The two-layer ONIOM method was used for QM/MM simulations of solid state, where the centroid molecule was chosen as QM region (high layer) and the remaining molecules were treated as MM region (low layer). The UFF force field was used for the MM expressions. The normal mode analyses were done with the help of the DUSHIN program.

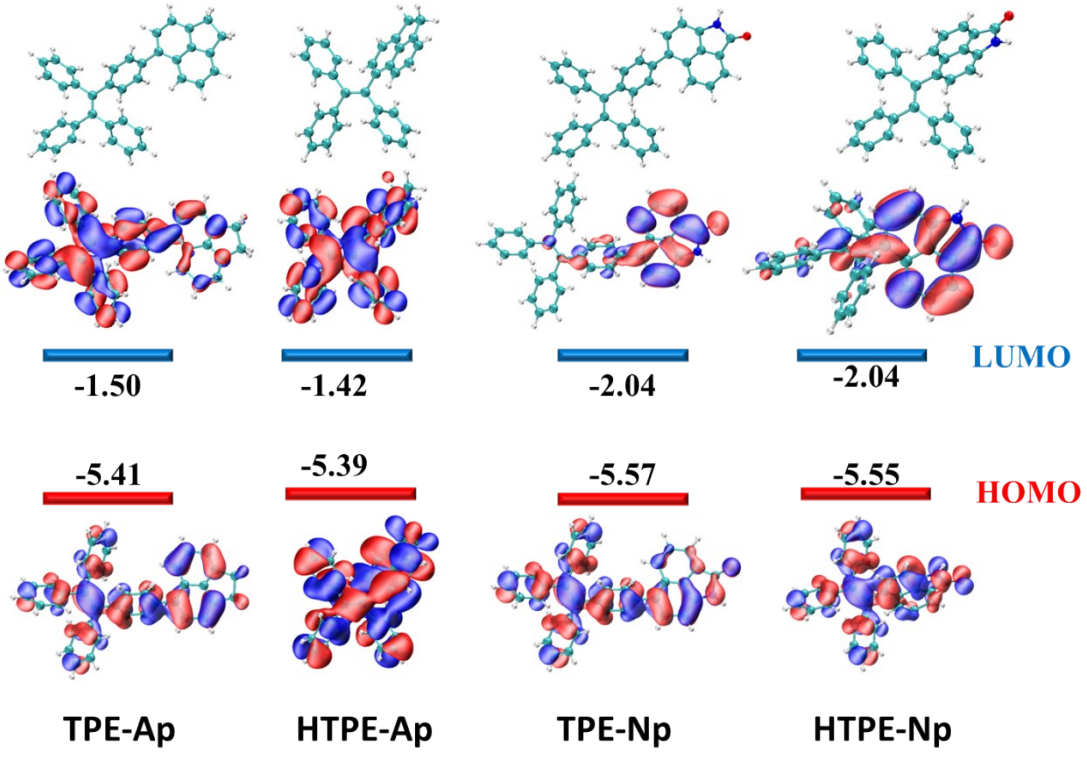

Figure S19. Calculated molecular structures and their orbital energy levels of **TPE-Ap**, **HTPE-Ap**, **TPE-Np** and **HTPE-Np**, unit: eV.

Table S3. The selected structure parameters of four compounds both in ground and exits states, and the calculated reorganization energy.

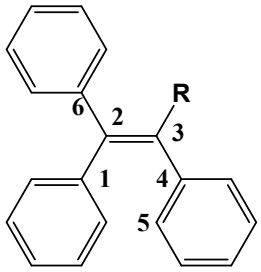

∠A = φ1-2-3-4； ∠B = φ2-3-4-5； ∠C = ∠1-2-6

Sample		S0			S1			λ[a]
		∠A	∠B	∠C	∠A	∠B	∠C	
TPE-Np	Dimer	10.64	48.16	114.55	16.16	47.38	115.79	6.21
	Monomer	10.65	49.07	114.54	17.11	42.73	115.95	14.48
	Solid state	3.98	32.79	114.23	15.19	40.88	119.28	5.23
	Experiment	5.63	37.71	114.08	--	--	--	--
HTPE-Np	Dimer	11.19	46.42	114.58	24.59	39.23	117.51	7.61
	Monomer	10.52	44.98	114.51	20.65	40.90	117.10	16.37
	Solid state	6.74	34.89	114.69	12.14	25.18	112.54	5.87
	Experiment	8.90	39.56	114.78	--	--	--	--
TPE-Ap	Monomer	10.66	48.96	114.53	29.23	31.42	119.85	16.56
	Solid state	0.62	10.47	112.05	13.16	30.26	116.13	4.47
	Experiment	5.47	55.00	114.04	--	--	--	--
HTPE-Ap	Monomer	9.99	43.92	114.50	35.37	33.70	120.68	17.24
	Solid state	19.42	55.19	114.50	21.71	36.24	116.86	4.80
	Experiment	12.75	19.73	114.05	--	--	--	--

[a] reorganization energy (unit: kcal/mol)

Table S4. Calculated Vertical Transition Energy, Emission Energy, Oscillator Strength (f) for four compounds in both solution and solid phases.

	Absorption	Emission
TPE-Np	334 nm (f = 0.1984) HOMO-1→ LUMO (47%) HOMO→ LUMO +1 (50%)	413 nm (f = 0.2741) LUMO→HOMO-1 (18%) LUMO+1→HOMO (67%)
HTPE-Np	343 nm (f = 0.1998) HOMO-1 → LUMO (28%) HOMO → LUMO +1 (63%)	429 nm (f = 0.2532) LUMO→HOMO-1 (13%) LUMO+1→HOMO (72%)
TPE-Ap	348 nm (f = 0.2723) HOMO-1 → LUMO (67%) HOMO → LUMO +1 (20%)	443 nm (f = 0.3265) LUMO → HOMO-1 (69%) LUMO+1 → HOMO (13%)
HTPE-Ap	347 nm (f= 0.3008) HOMO-1→LUMO (42%) HOMO → LUMO +1 (55%)	410 nm (f = 0.2855) LUMO → HOMO-1 (39%) LUMO + 1 → HOMO (57%)
DTPE-Np	413nm (f = 0.6836) HOMO-1 → LUMO (44%) HOMO → LUMO +1(54%)	559 nm (f = 0.3814) LUMO → HOMO-1 (70%) LUMO + 1→ HOMO (15%)
DHTPE-Np	432 nm (f = 0.4210) HOMO-1→ LUMO (45%) HOMO→ LUMO +1 (53%)	490 nm (f = 0.4163) LUMO → HOMO-1 (45%) LUMO + 1→ HOMO (53%)

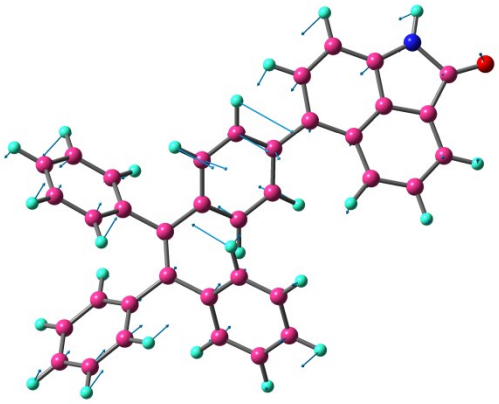

122 cm^{-1}

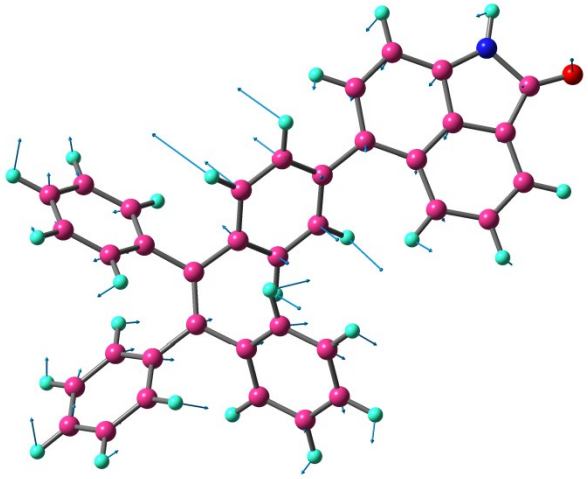

145 cm^{-1}

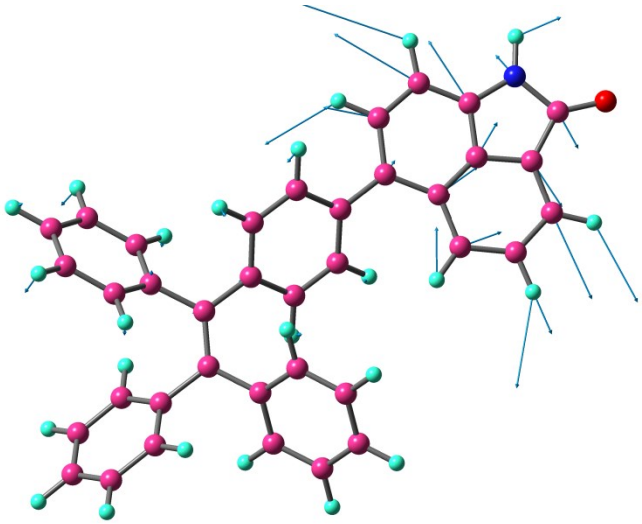

569 cm^{-1}

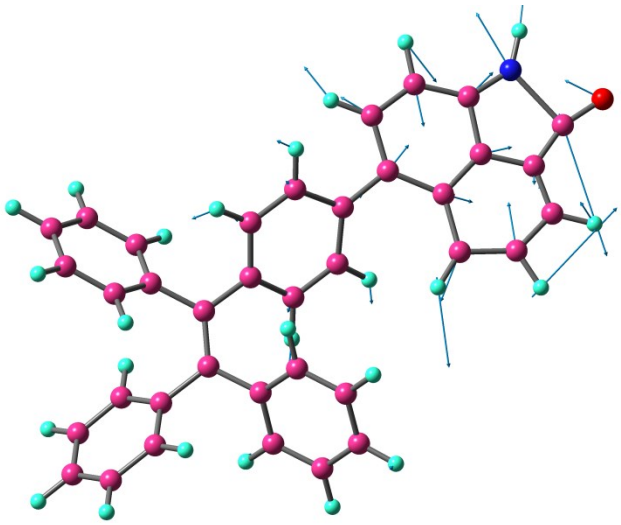

937 cm^{-1}

Figure S20. Scheme for the normal mode displacement vectors of monomer **TPE-Np** for vibrations at 122 and 145 cm^{-1} (side ring twisting) and 569 and 973 cm^{-1} (double bond stretching of Np group).

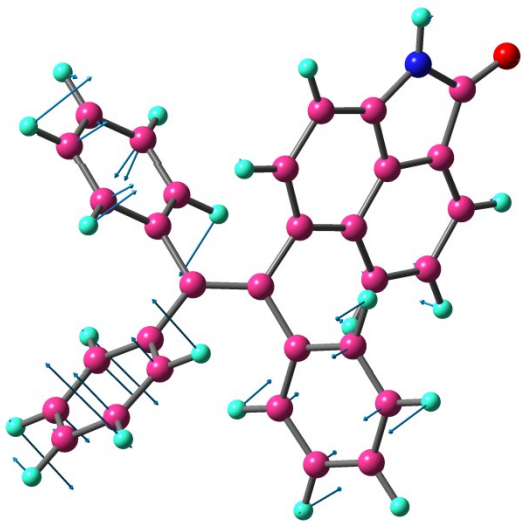

103 cm^{-1}

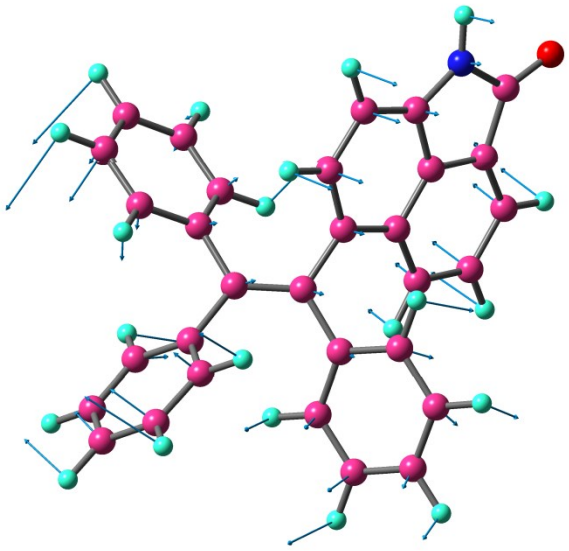

68 cm^{-1}

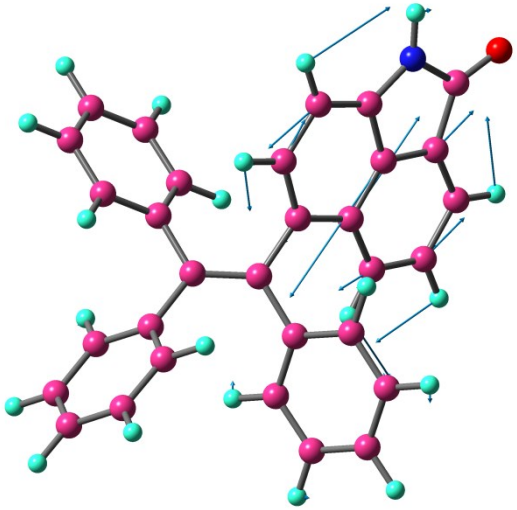

1630 cm^{-1}

Figure S21. Scheme for the normal mode displacement vectors of monomer **HTPE-Np** for vibrations at 68 and 103 cm^{-1} (side ring twisting) and 1630 cm^{-1} (double bond stretching of Np group).

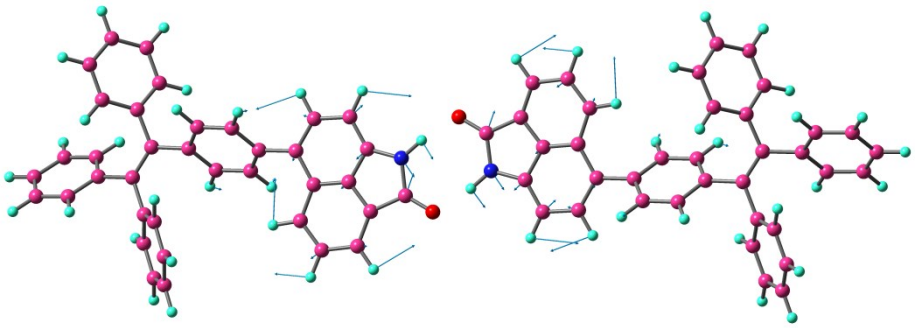

1072 cm^{-1}

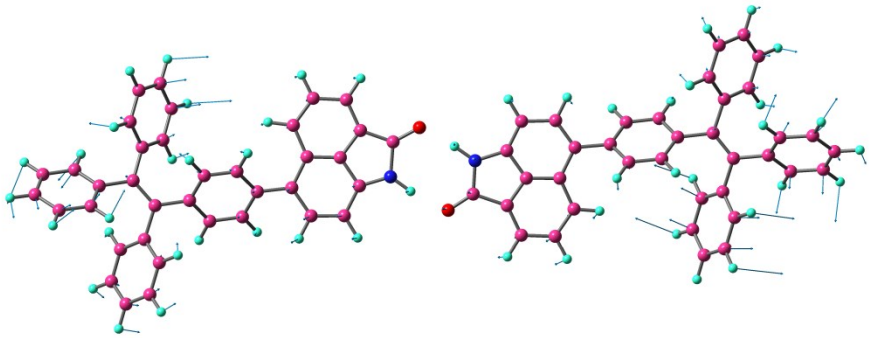

85 cm^{-1}

Figure S22. Scheme for the normal mode displacement vectors of dimer **TPE-Np** for vibrations at 85 cm^{-1} (side ring twisting) and 1072 cm^{-1} (double bond stretching of Np group).

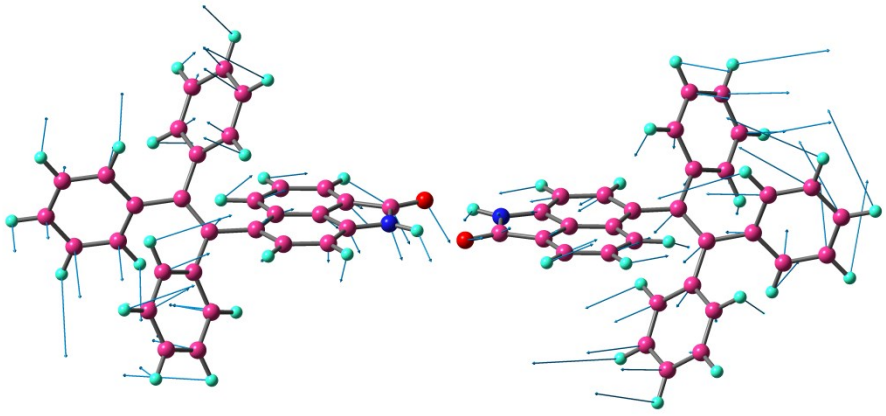

44 cm^{-1}

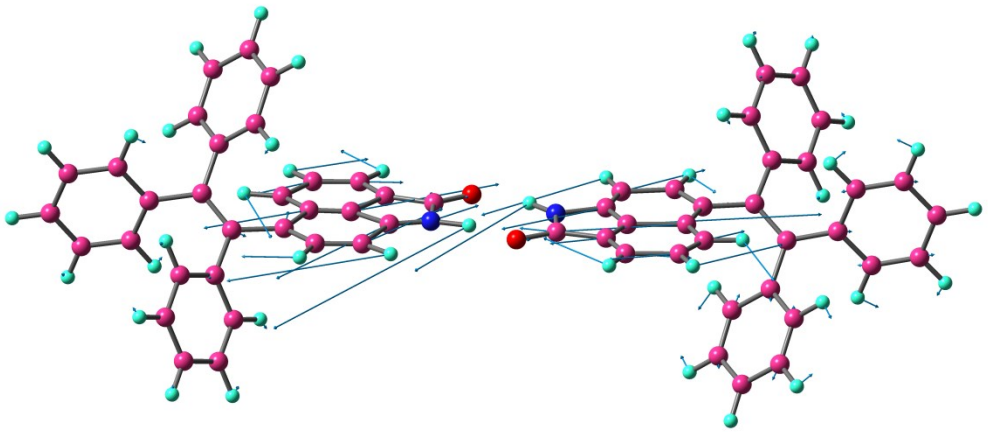

1630 cm^{-1}

Figure S23. Scheme for the normal mode displacement vectors of monomer **HTPE-Np** for vibrations at 44 cm^{-1} (side ring twisting) and 1630 cm^{-1} (double bond stretching of Np group).

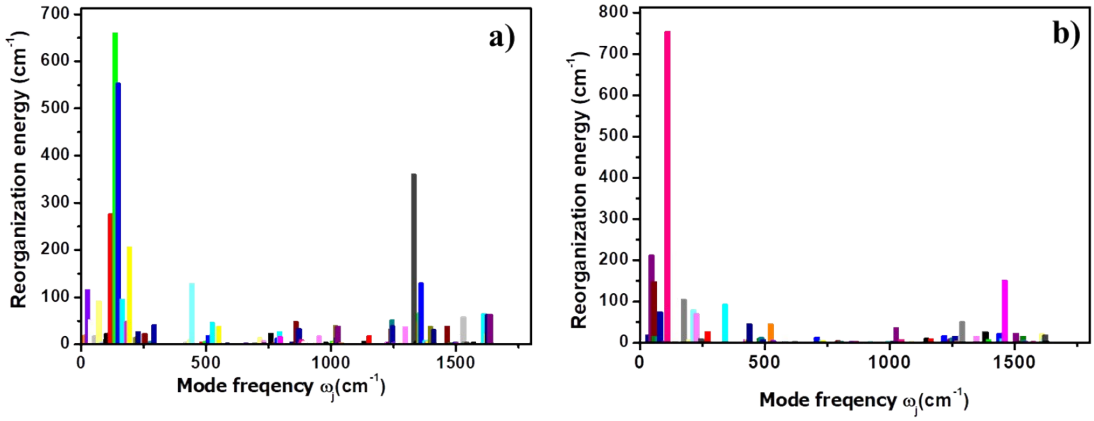

Figure S24. Plots of calculated reorganization energy versus the normal mode wavenumber of a) **TPE-Ap** and b) **HTPE-Ap**.

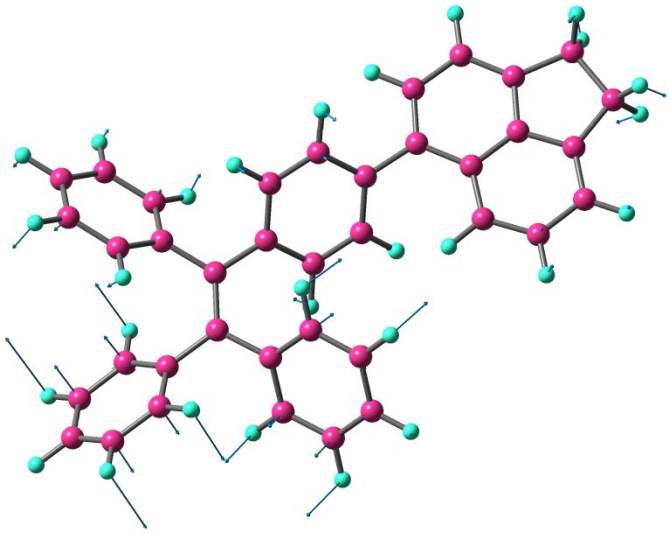

107 cm^{-1}

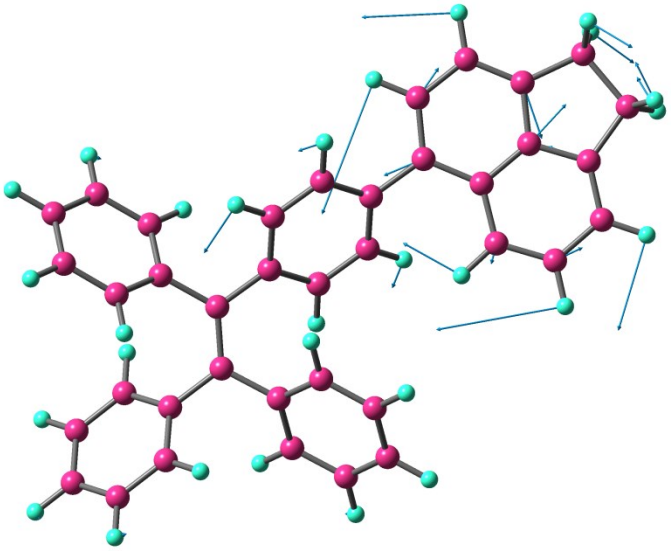

1450 cm^{-1}

Figure S25. Scheme for the normal mode displacement vectors of monomer **HTPE-Np** for vibrations at 107 cm^{-1} (side ring twisting of TPE) and 1450 cm^{-1} (double bond stretching of Ap group).

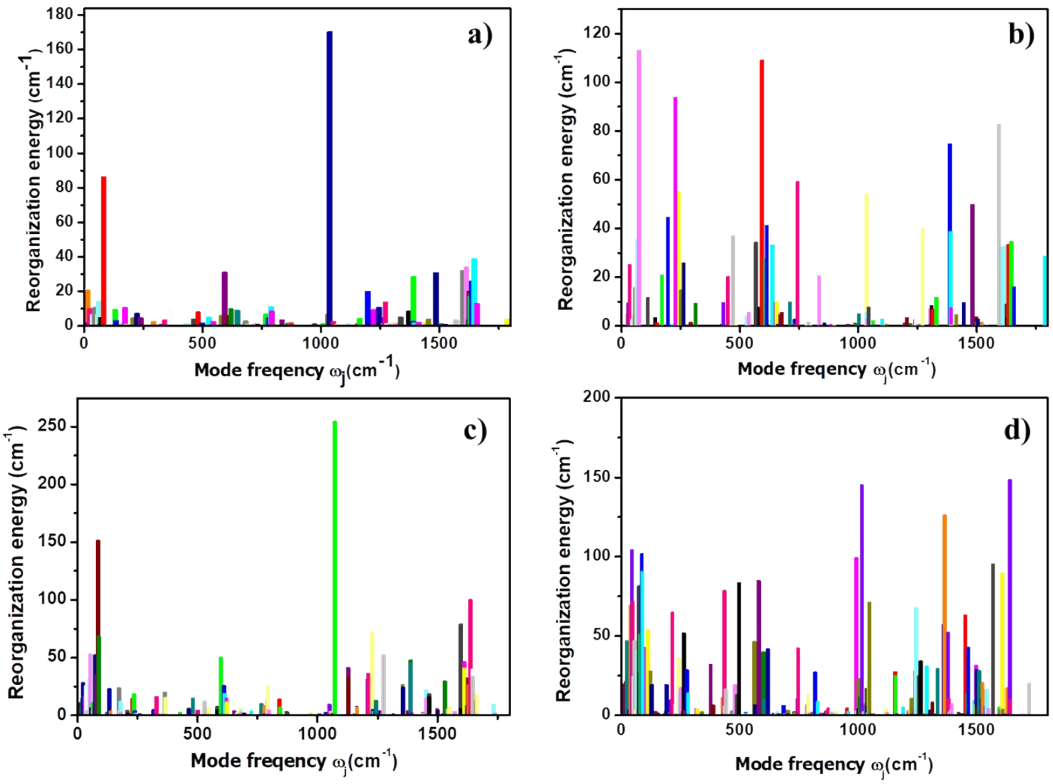

Figure S26. Plots of calculated reorganization energy versus the normal mode wavenumber of a) **TPE-Np**, b) **TPE-Ap**, c) **HTPE-Np** and d) **HTPE-Ap** in solid states.

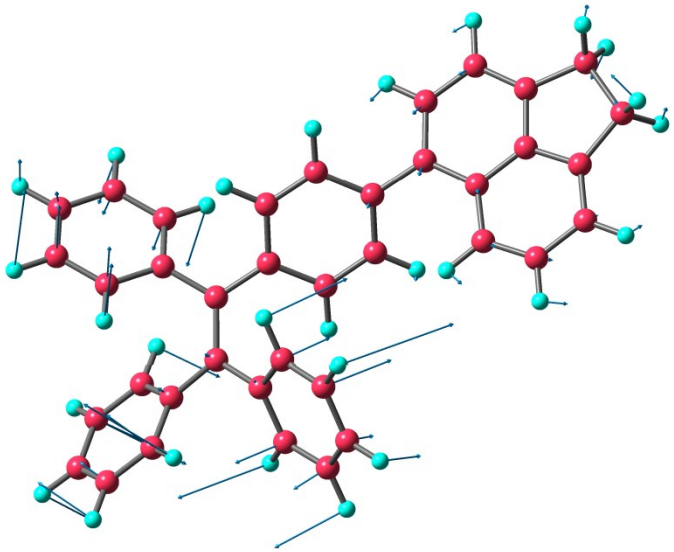

100.79 cm^{-1}

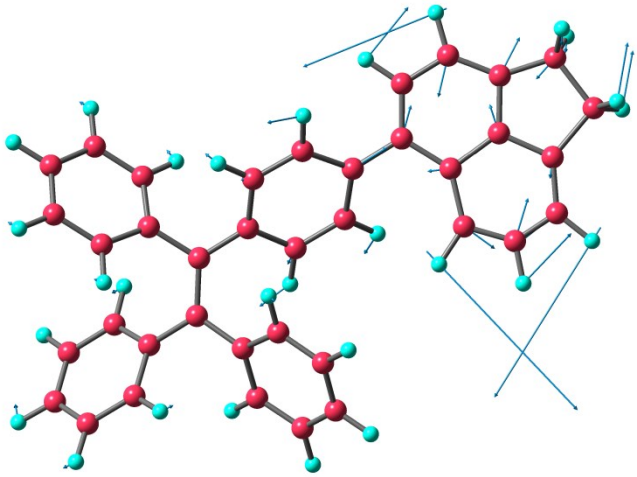

1098 cm^{-1}

Figure S27. Scheme for the normal mode displacement vectors of **TPE-Ap** in solid tates for vibrations at 101 cm^{-1} (side ring twisting of TPE) and 1098 cm^{-1} (double bond stretching of Ap group).

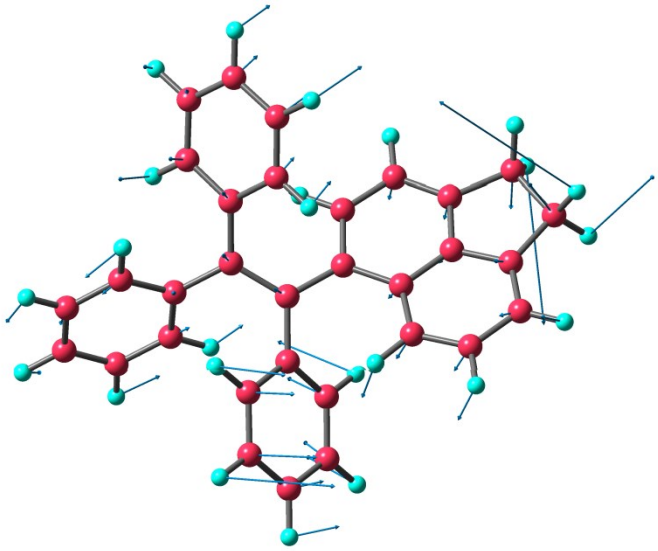

94 cm^{-1}

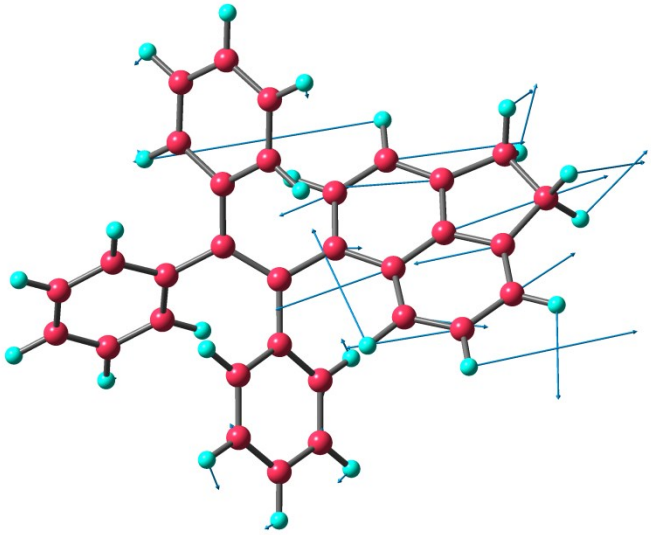

1627 cm^{-1}

Figure S28. Scheme for the normal mode displacement vectors of **HTPE-Ap** in solid states for vibrations at 94 cm^{-1} (side ring twisting of TPE) and 1627 cm^{-1} (double bond stretching of Ap group).

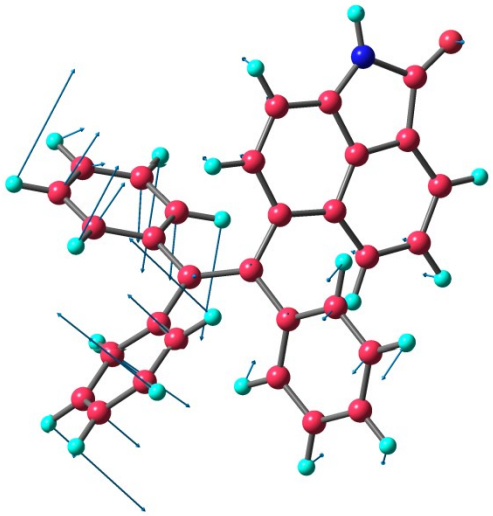

102 cm^{-1}

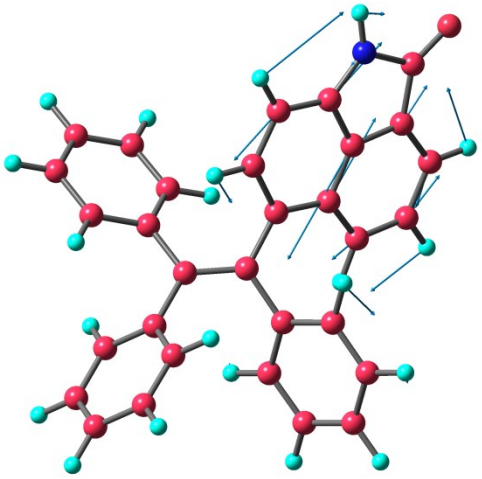

1644 cm^{-1}

Figure S29. Scheme for the normal mode displacement vectors of **HTPE-Np** in solid states for vibrations at 102 cm^{-1} (side ring twisting of TPE) and 1644 cm^{-1} (double bond stretching of Ap group).

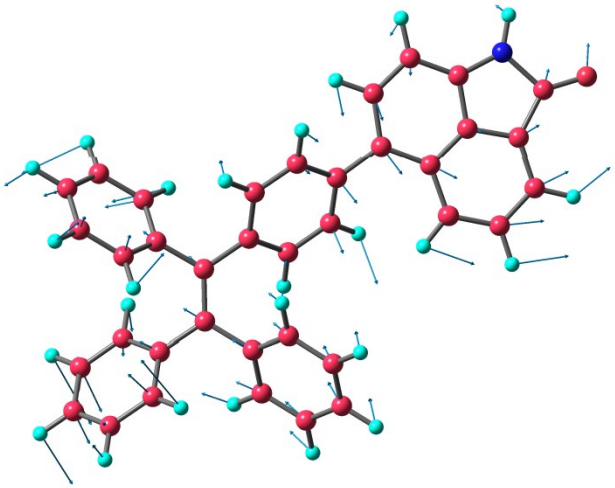

76 cm^{-1}

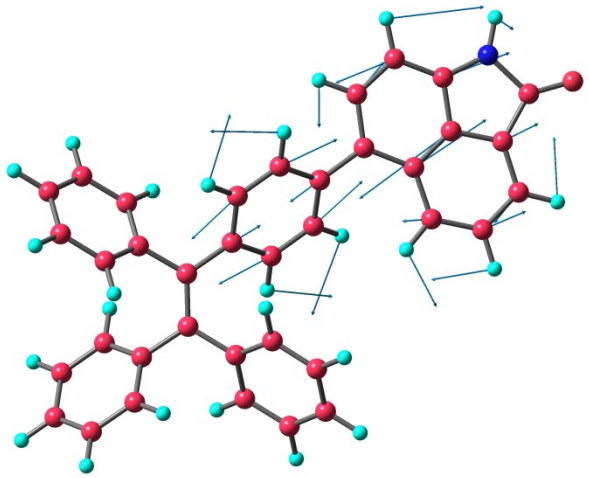

1629 cm^{-1}

Figure S30. Scheme for the normal mode displacement vectors of **TPE-Np** in solid states for vibrations at 76 cm^{-1} (side ring twisting of TPE) and 1629 cm^{-1} (double bond stretching of Ap group).

6. ^{1}H NMR, ^{13}C NMR and MS spectra

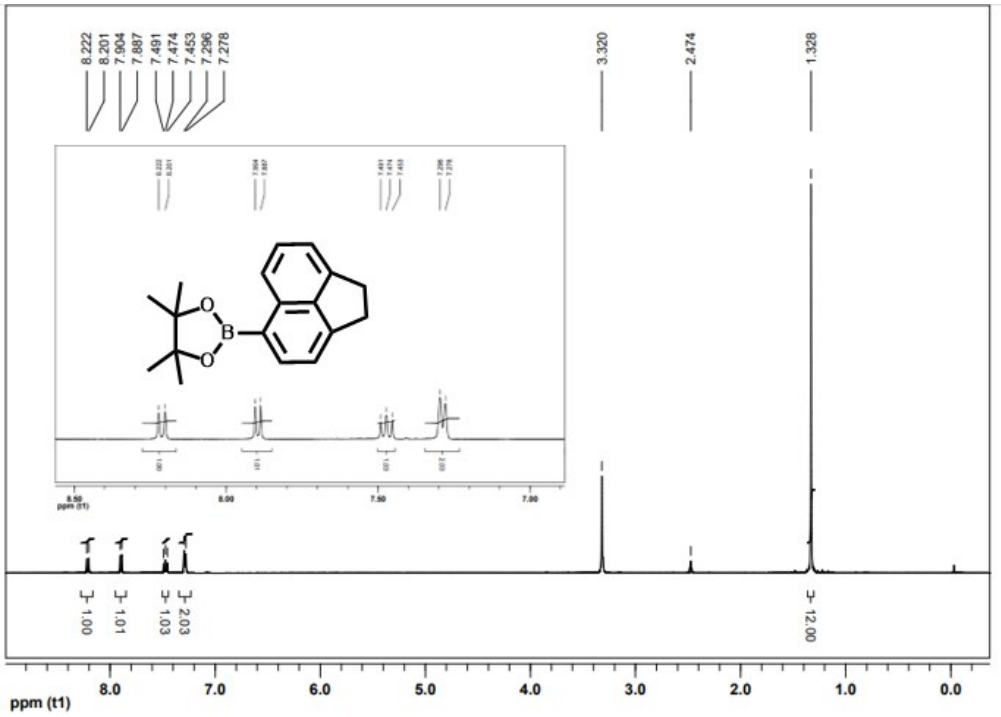

Figure S31. ^{1}H NMR spectrum of target **Bpin-Ap** in DMSO-d_6.

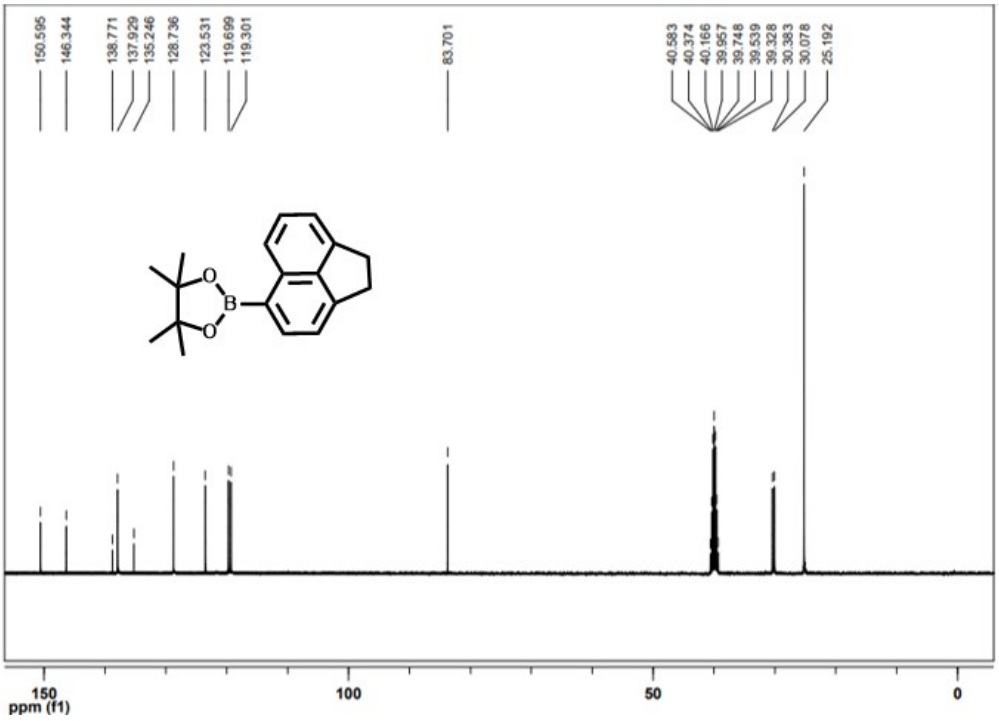

Figure S32. ^{13}C NMR spectrum of target **Bpin-Ap** in DMSO-d_6.

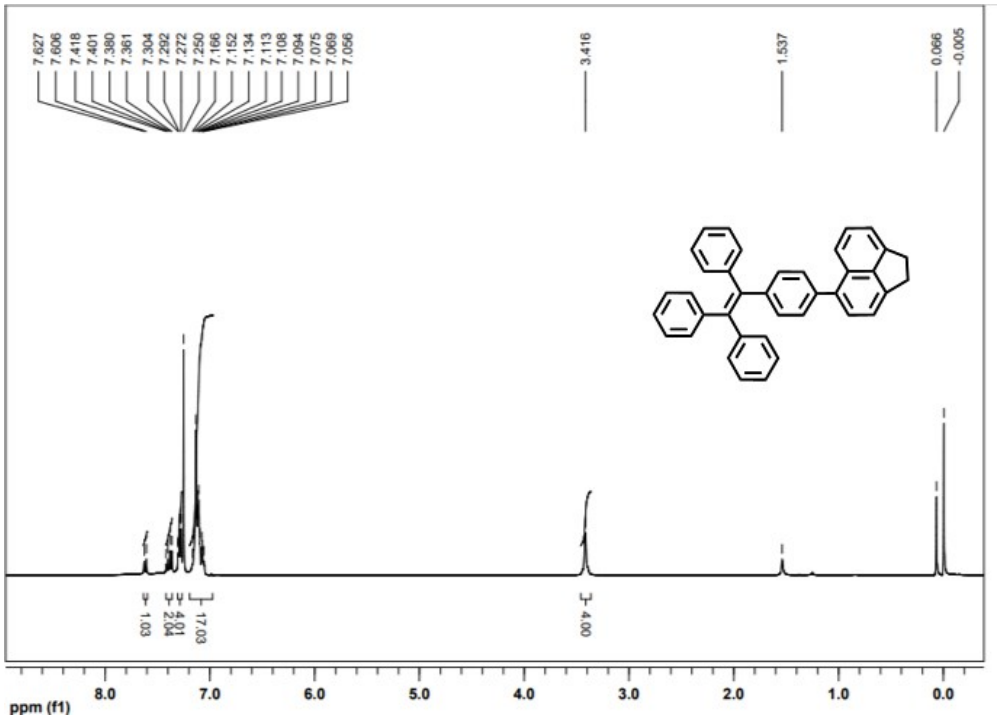

Figure S33. ^{1}H NMR spectrum of target **TPE-Ap** in $CDCl_3$.

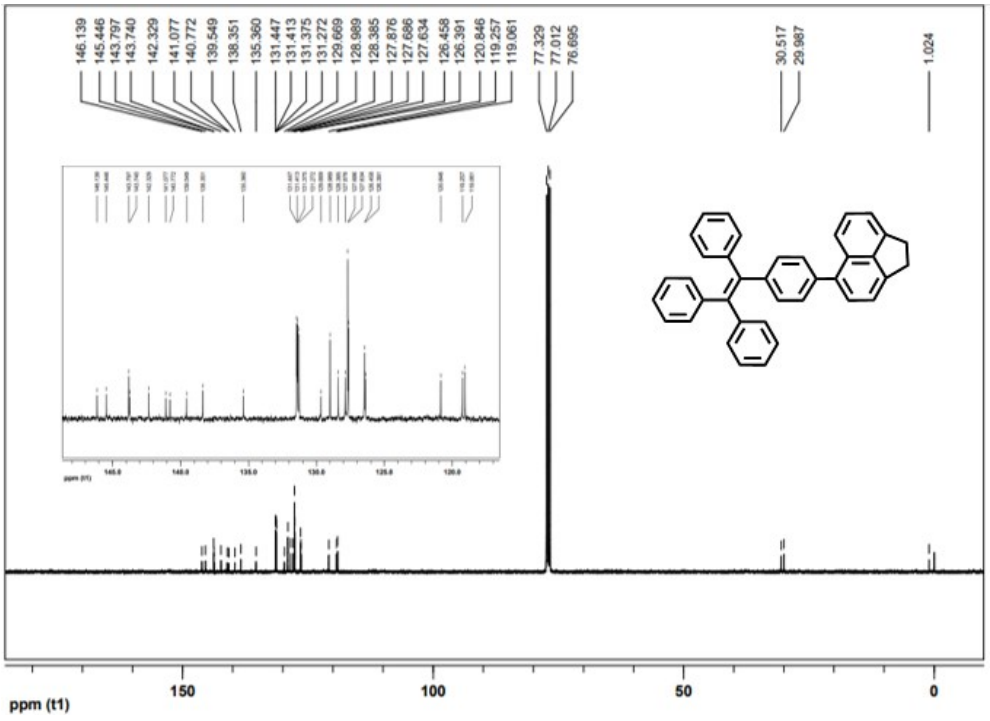

Figure S34. ^{13}C NMR spectrum of target **TPE-Ap** in $CDCl_3$.

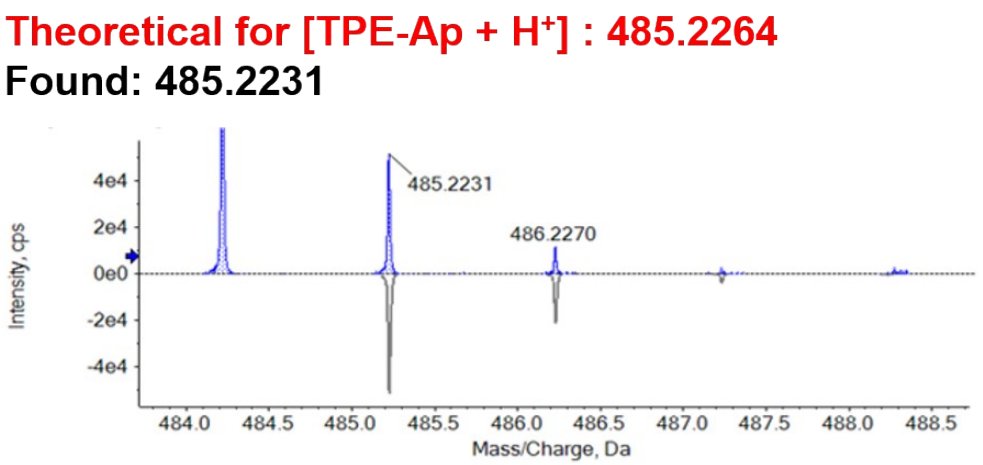

Figure S35. Mass spectrum of target **TPE-Ap**.

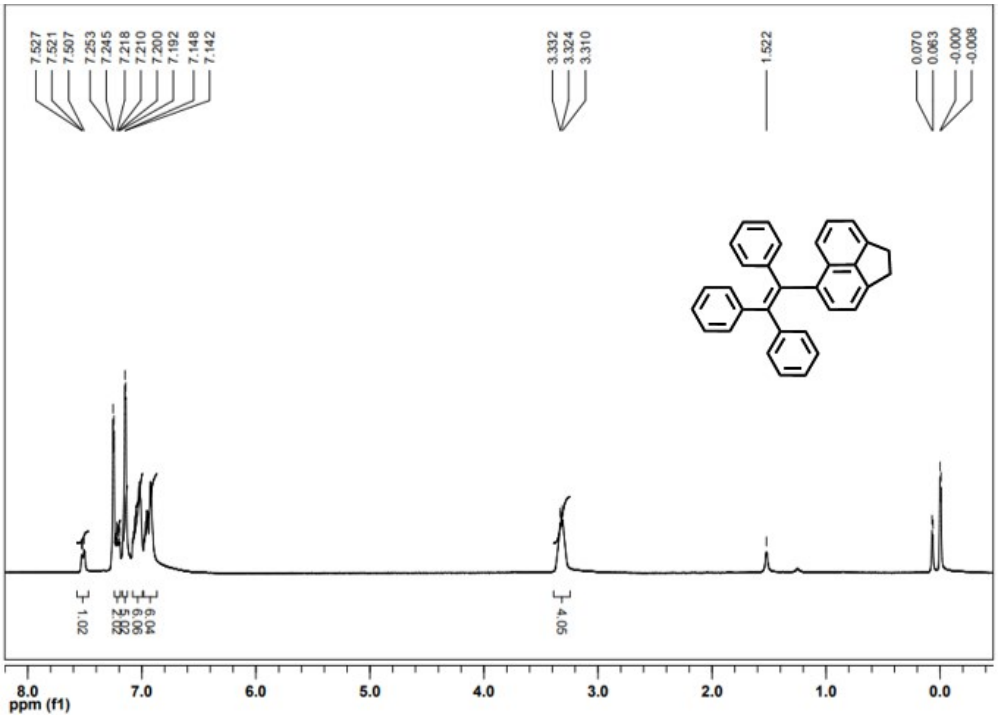

Figure S36. ^{1}H NMR spectrum of target **HTPE-Ap** in $CDCl_3$.

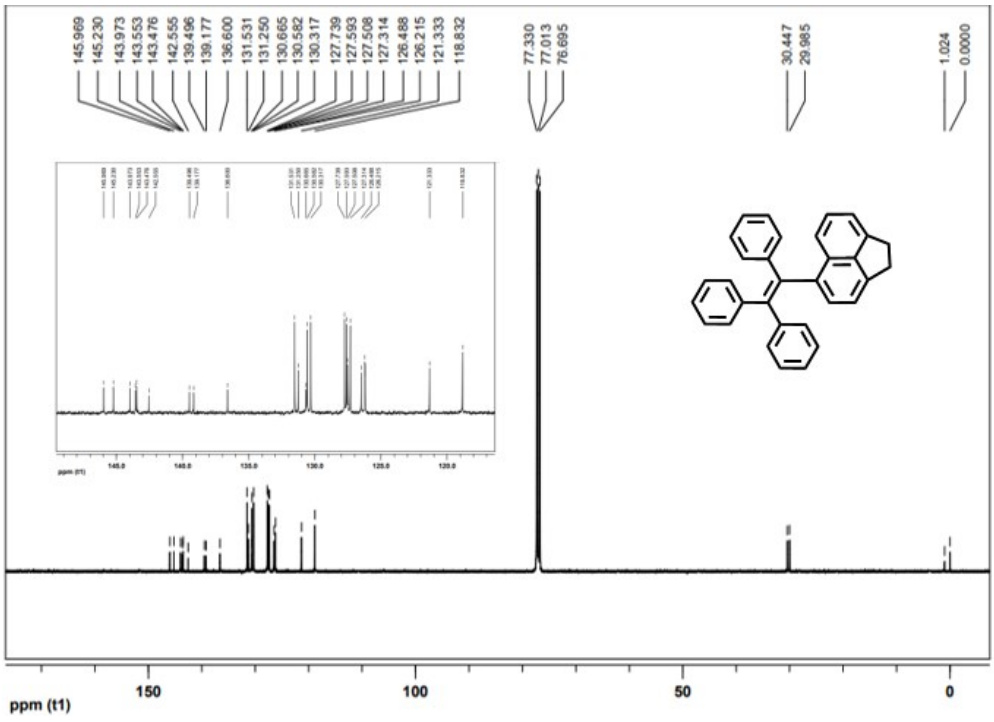

Figure S37. ^{13}C NMR spectrum of target **HTPE-Ap** in $CDCl_3$.

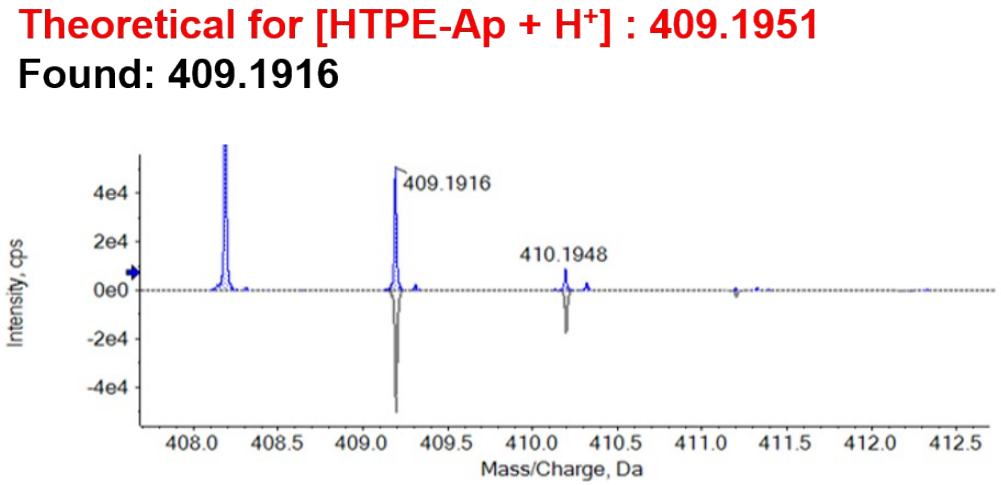

Figure S38. Mass spectrum of target **HTPE-Ap**.

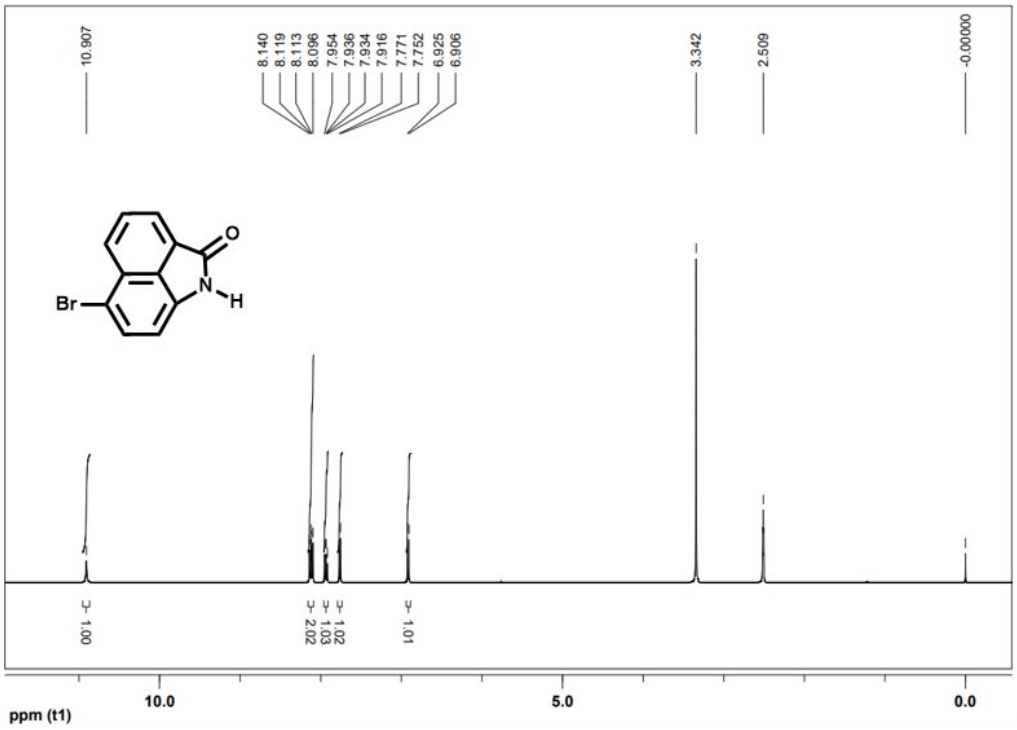

Figure S39. ^{1}H NMR spectrum of target **Br-Np** in DMSO-d_6.

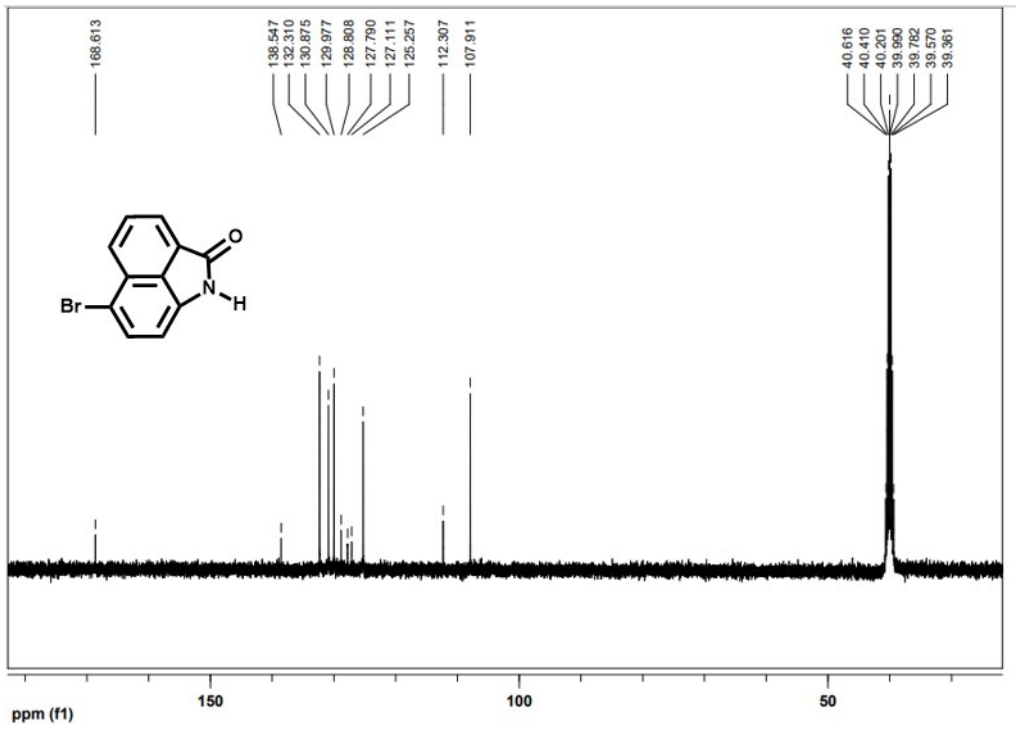

Figure S40. ^{13}C NMR spectrum of target **Br-Np** in DMSO-d_6.

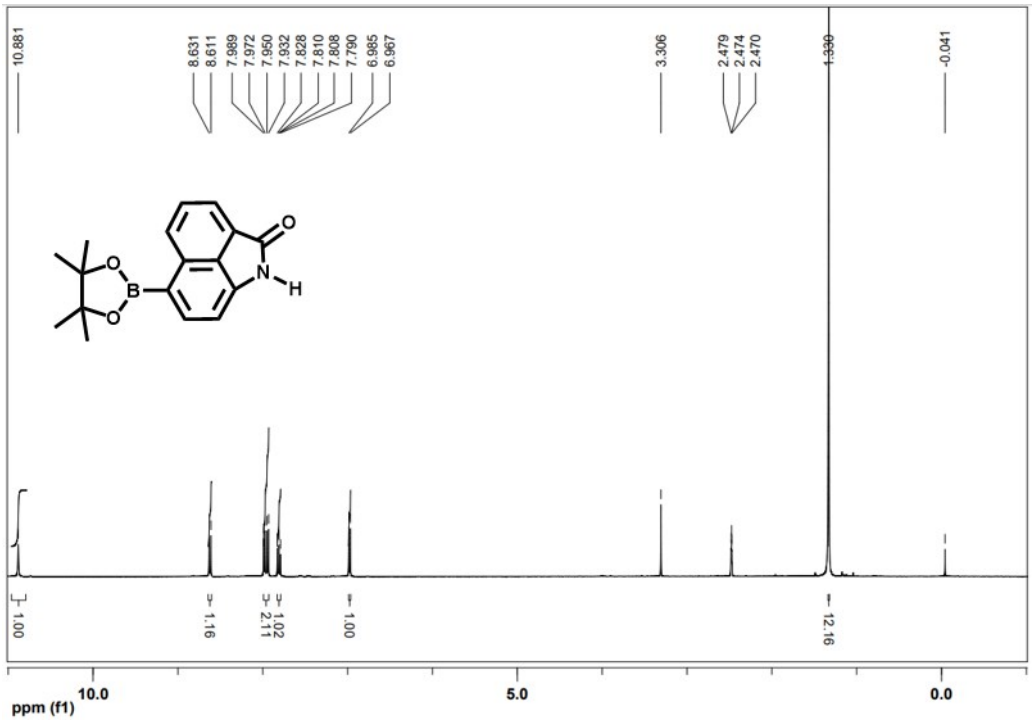

Figure S41. ^{1}H NMR spectrum of target **Pin-Np** in DMSO-d_6.

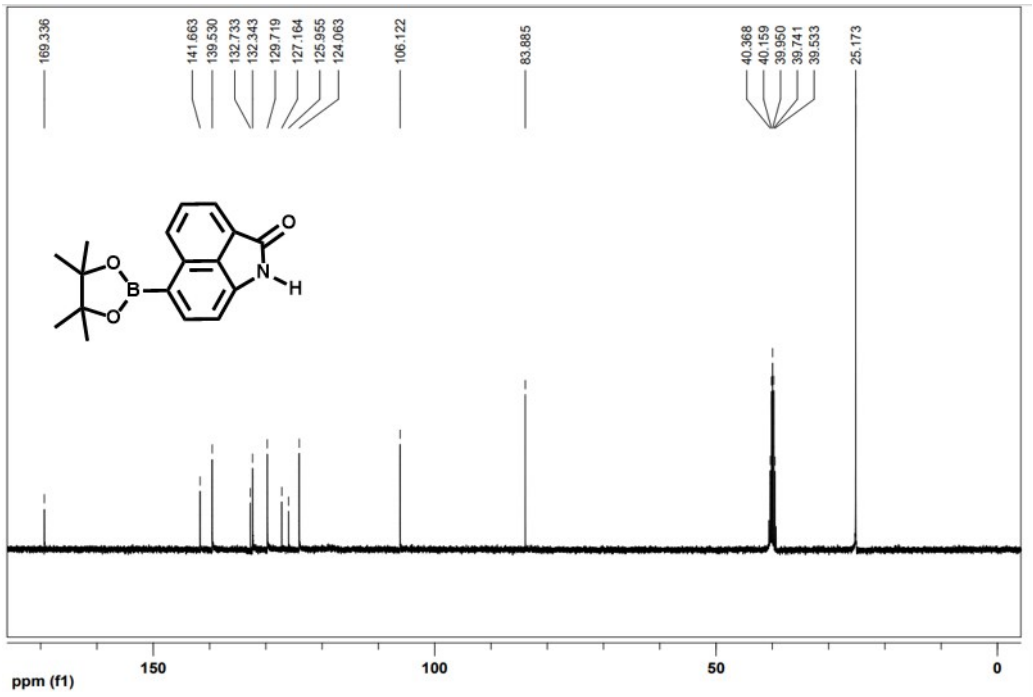

Figure S42. ^{13}C NMR spectrum of target **Pin-Np** in DMSO-d_6.

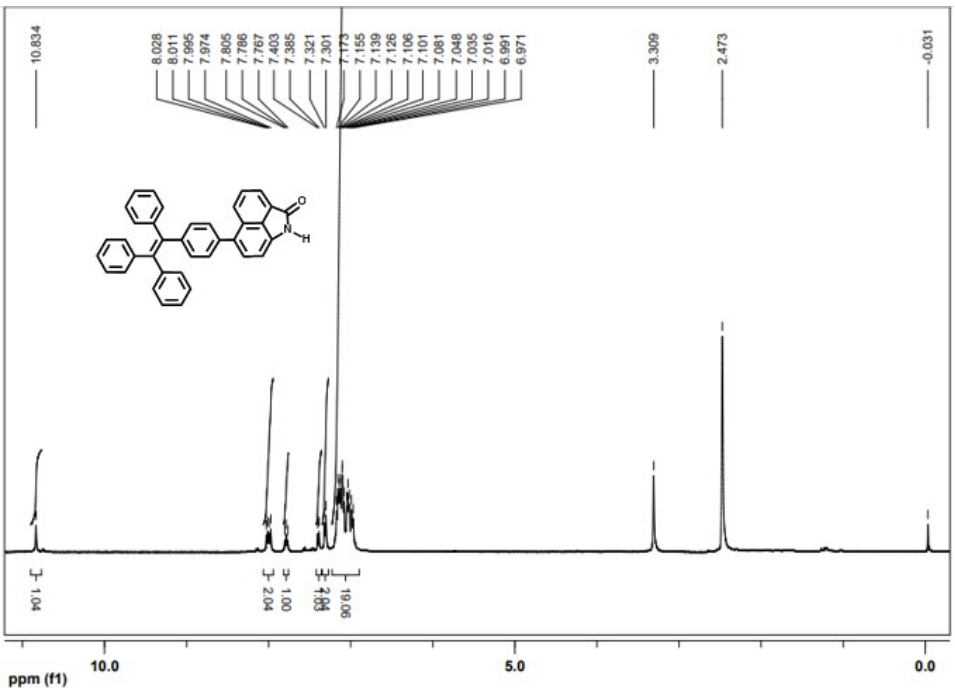

Figure S43. ^{1}H NMR spectrum of target **TPE-Np** in DMSO-d_6.

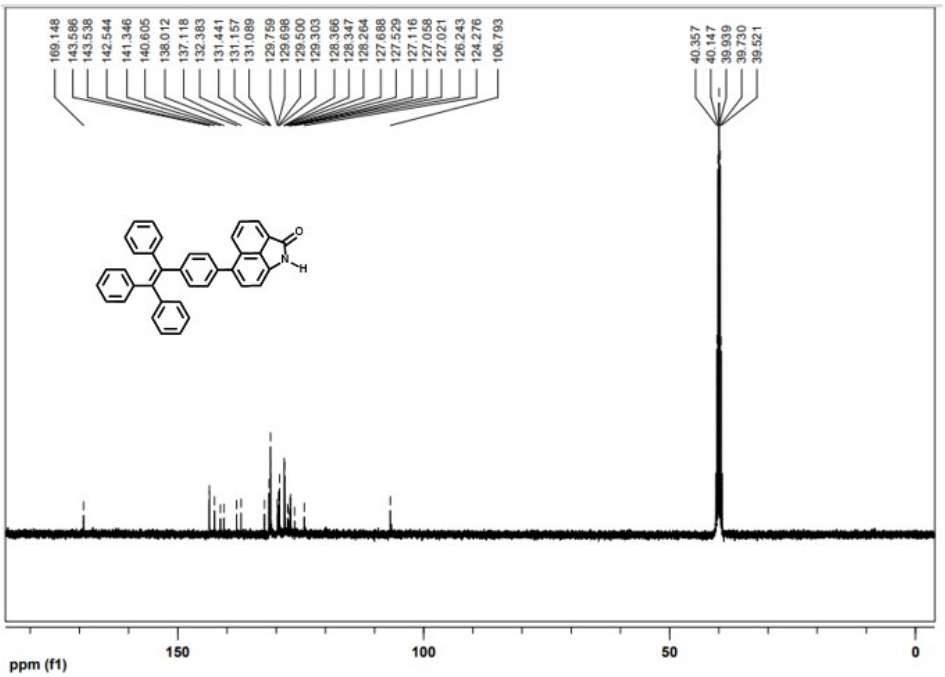

Figure S44. ^{13}C NMR spectrum of target **TPE-Np** in DMSO-d_6.

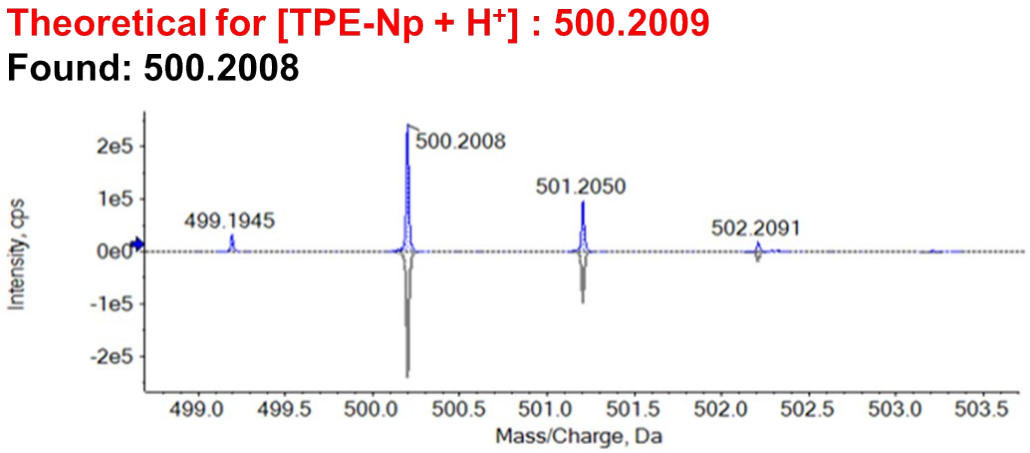

Figure S45. Mass spectrum of target **TPE-Np**.

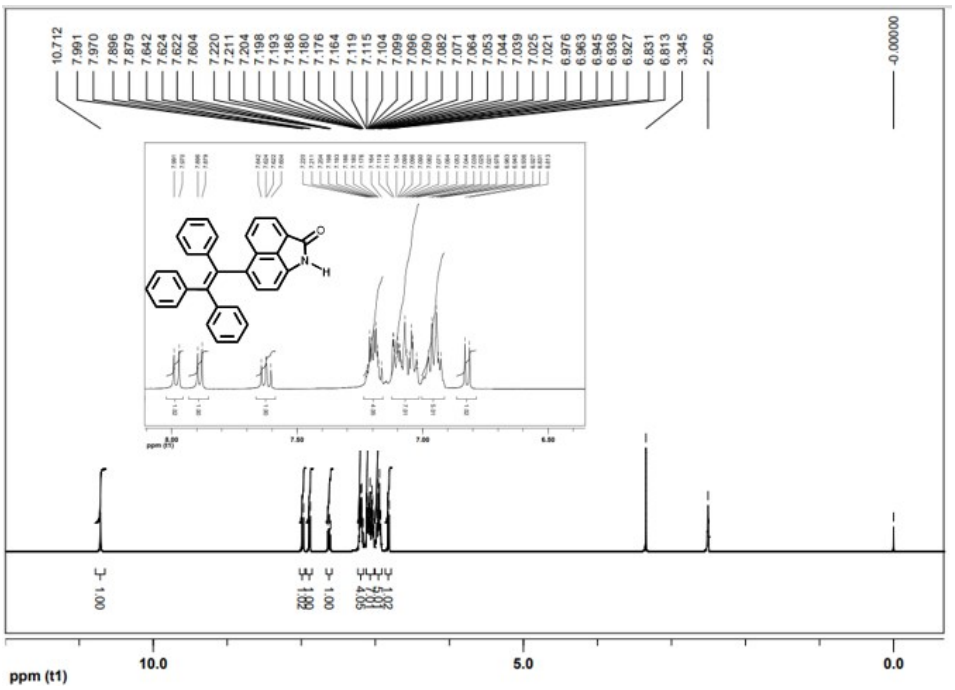

Figure S46. ^{1}H NMR spectrum of target **HTPE-Np** in DMSO-d_6.

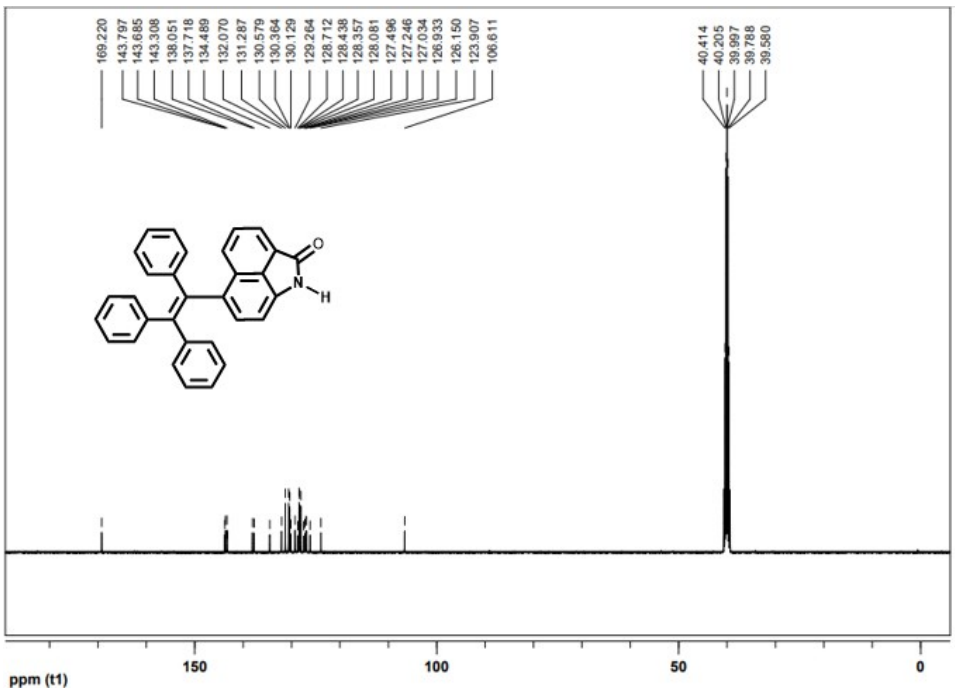

Figure S47. ^{13}C NMR spectrum of target **HTPE-Np** in DMSO-d_6.

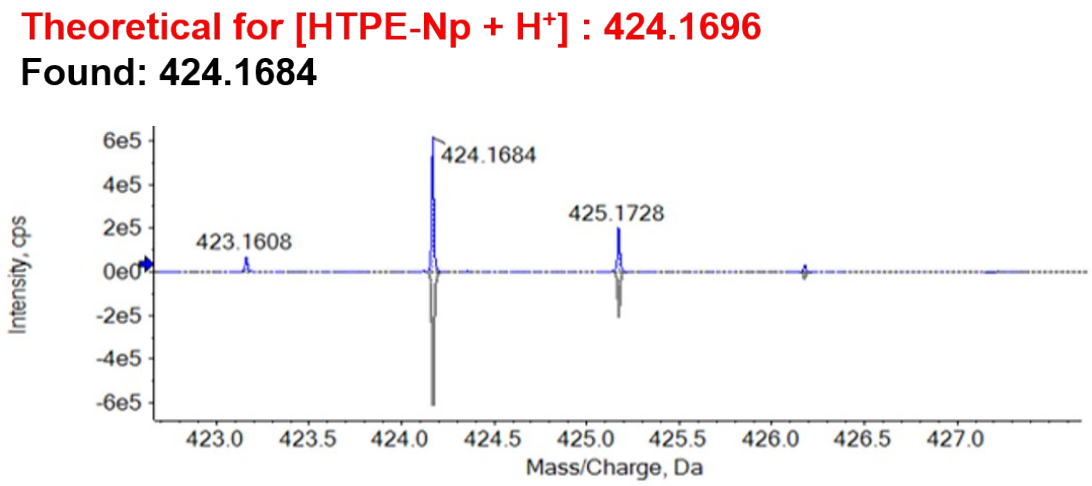

Figure S48. Mass spectrum of target **HTPE-Np**.

7. Reference

[1] Y. Haishima, Y. Kubota, K. Manseki, J. Jin, Y. Sawada, T. Inuzuka, K. Funabiki, M. Matsui, *J. Org. Chem.* 2018, **83**, 4389.

[2] M. J. Frisch, G. W. Trucks, H. B. Schlegel, G. E. Scuseria, M. A. Robb, J. R. Cheeseman, G. Scalmani, V. Barone, B. Mennucci, G. A. Petersson, H. Nakatsuji, M. Caricato, X. Li, H. P. Hratchian, A. F. Izmaylov, J. Bloino, G. Zheng, J. L. Sonnenberg, M. Hada, M. Ehara, K. Toyota, R. Fukuda, J. Hasegawa, M. Ishida, T. Nakajima, Y. Honda, O. Kitao, H. Nakai, T. Vreven, J. A. Montgomery, Jr., J. E. Peralta, F. Ogliaro, M. Bearpark, J. J. Heyd, E. Brothers, K. N. Kudin, V. N. Staroverov, R. Kobayashi, J. Normand, K. Raghavachari, A. Rendell, J. C. Burant, S. S. Iyengar, J. Tomasi, M. Cossi, N. Rega, J. M. Millam, M. Klene, J. E. Knox, J. B. Cross, V. Bakken, C. Adamo, J. Jaramillo, R. Gomperts, R. E. Stratmann, O. Yazyev, A. J. Austin, R. Cammi, C. Pomelli, J. W. Ochterski, R. L. Martin, K. Morokuma, V. G. Zakrzewski, G. A. Voth, P. Salvador, J. J. Dannenberg, S. Dapprich, A. D. Daniels, Ö. Farkas, J. B. Foresman, J. V. Ortiz, J. Cioslowski, and D. J. Fox, Gaussian 16, Revision B.01, GaussianInc., Wallingford CT, 2016.

[3] S. Dapprich, I. Komáromi, K. S. Byun, K. Morokuma and M. J. Frisch, *J. Mol. Struct. (Theochem)* 1999, **461**, 1-21.

[4] J. R. Reimers, *J. Chem. Phys.* 2001, **115**, 9103-9109.